

000 001 002 003 004 005 006 007 008 009 010 011 012 013 014 015 016 017 018 019 020 021 022 023 024 025 026 027 028 029 030 031 032 033 034 035 036 037 038 039 040 041 042 043 044 045 046 047 048 049 050 051 052 053 STATISTICAL AND STRUCTURAL IDENTIFIABILITY IN SELF-SUPERVISED LEARNING

Anonymous authors

Paper under double-blind review

ABSTRACT

Self-supervised models exhibit a surprising stability in their internal representations. Whereas most prior work treats this stability as a single property, we formalize it as two distinct concepts: **statistical identifiability** (consistency of representations across runs) and **structural identifiability** (alignment of representations with some unobserved ground truth). Recognizing that perfect pointwise identifiability is generally unrealistic for modern representation learning models, we propose new model-agnostic definitions of statistical and structural near-identifiability of representations up to some error tolerance ϵ . Leveraging these definitions, we prove a statistical ϵ -near-identifiability result for the representations of models with nonlinear decoders, generalizing existing identifiability theory beyond last-layer representations in e.g. generative pre-trained transformers (GPTs) to near-identifiability of the intermediate representations of a broad class of models including (masked) autoencoders (MAEs) and supervised learners. Although these weaker assumptions confer weaker identifiability, we show that independent components analysis (ICA) can resolve much of the remaining linear ambiguity for this class of models, and validate and measure our near-identifiability claims empirically. With additional assumptions on the data-generating process, statistical identifiability extends to **structural identifiability**, yielding a simple and practical recipe for disentanglement: ICA post-processing of latent representations. On synthetic benchmarks, this approach achieves state-of-the-art disentanglement using a vanilla autoencoder. With a foundation model-scale MAE for cell microscopy, it disentangles biological variation from technical batch effects, substantially improving downstream generalization.

1 INTRODUCTION

Despite the massive variety of data modalities, pretext tasks, training procedures, and datasets, disparate self-supervised learning models as a whole seem to be converging on a shared set of representations of the natural world (Huh et al., 2024) which are useful for a surprising variety of downstream tasks (Kraus et al., 2024; Hayes et al., 2025; Baevski et al., 2020; Brohan et al., 2023). A classical lens for studying this phenomenon is the notion of *identifiability* (Reizinger et al., 2025a). In likelihood-based statistical inference, identifiability is the condition that data are sufficient to completely characterize the parameters of the model (Casella & Berger, 2001). The situation is considerably trickier for neural network models: the parameter space is large and invariant to e.g. permutations of the neurons, and the training procedures might lack a likelihood-based interpretation. Instead, recent work in identifiability focuses on finding conditions such that infinite data is sufficient to characterize the trained model’s *representations* of that data (Reizinger et al., 2025a) up to some equivalence class such as a linear transformation (Roeder et al., 2021).

We begin by sharpening existing definitions of representation identifiability, recognizing that existing results fall into two categories. The first is what we refer to as **statistical identifiability**, or the condition that optimizing a given representation learning model will yield the *same* representations up to some simple transformation. The second is what we refer to as **structural identifiability**, or the condition that optimizing a given representation learning model will yield a *particular* representation every time, corresponding to some latent component of the data-generating process. We provide definitions of statistical and structural identifiability that relax the requirement that the representations are exactly identifiable, making them the first general-purpose formulations which are applicable to

054 the case where the representations are “nearly” identifiable up to some error tolerance ϵ and extending
 055 prior model-specific cases (Nielsen et al., 2025; Buchholz & Schölkopf, 2024).
 056

057 Leveraging these definitions, we prove several new identifiability results. Our first result shows that
 058 for models which have statistically identifiable outputs, such as generative pre-trained transformers,
 059 supervised classifiers, and encoder-decoder models (Roeder et al., 2021), the *intermediate-layer*
 060 representations are also statistically ϵ -nearly identifiable up to a rigid transformation. Unlike several
 061 recent results, these representations can be mapped non-linearly to the loss, and ϵ is governed
 062 by a mild function class condition on the mapping from the intermediate layer to the identifiable
 063 outputs. Our second result shows that linear independent components analysis (ICA) can resolve this
 064 rigid indeterminacy, yielding near-identifiability up to signed permutations. Notably, our sharper
 065 definitions of statistical and structural identifiability reveal that these results are available without
 066 strong assumptions on the data-generating process, instead requiring only this mild function class
 067 assumption on the model. Our final result shows that if one is willing to make a similar assumption on
 068 the data-generating process, encoder-decoder models which are statistically identifiable and achieve
 069 perfect reconstruction are also structurally identifiable. Notably, perfect reconstruction is another
 070 assumption which can be relaxed if statistical identifiability is all that is required.

071 In addition to our theoretical contributions, we perform a series of experiments to validate our claims.
 072 In synthetic experiments on autoencoders, we show that hyperparameter selection and regularization
 073 impacts the statistical identifiability nearness ϵ in ways that are predicted by our theory. Subsequent
 074 experiments show that near-identifiability also holds in off-the-shelf pre-trained models, and that the
 075 linear indeterminacies predicted by our theory can in practice be resolved by ICA. Next, we investigate
 076 whether our structural identifiability result can be applied to the special case of disentanglement
 077 (Locatello et al., 2020), finding that the simple combination of vanilla autoencoders and linear ICA
 078 applied to the latent space yields disentanglement on several benchmark datasets, competitive with
 079 some of the best existing models. Finally, we show that linear ICA applied to the latent space of a
 080 masked autoencoder for cell imaging successfully disentangles batch effects from biological variation,
 081 a key problem in the application of machine learning to biology.

082 2 RELATED WORK

083 **Statistical identifiability of representations** Prior representation identifiability results make strong
 084 assumptions on the data-generating process (Zimmermann et al., 2021; Reizinger et al., 2025b;
 085 Khemakhem et al., 2020b; Chen et al., 2024; Lachapelle et al., 2023) or assume a linear relationship
 086 between the representations and the loss (Roeder et al., 2021; Marconato et al., 2025; Nielsen et al.,
 087 2025), and generally do not distinguish between **statistical and structural** identifiability as we do
 088 here. Our work directly addresses this gap by proposing a concrete definition of statistical ϵ -near-
 089 identifiability which is provably met by the general-purpose models in widespread use today, with only
 090 mild assumptions on the model class and few assumptions on the data-generating process. We directly
 091 measure the consequences of our *statistical identifiability* results by assessing the ℓ_2 convergence
 092 of representations in real-world models, extending prior work on representation similarity (Roeder
 093 et al., 2021; Huh et al., 2024; Klabunde et al., 2025; Nielsen et al., 2025; Marconato et al., 2025).
 094 Nielsen et al. (2025) relaxes the identifiability theory of Roeder et al. (2021) for generative pre-trained
 095 transformers, showing that the Kullback-Leibler divergence on the next-token distribution fails to
 096 serve as a witness for differences in the penultimate-layer representations, and proves a sufficient
 097 condition for divergences that do, which could be viewed as a particular form of near-identifiability
 098 for a particular model class. Reizinger et al. (2024) formalizes ϵ -non-identifiability with respect to
 099 the KL divergence, showing that this failure generalizes beyond representational identifiability to
 100 other properties of interest for large language models. For a history of the term identifiability, see
 101 Appendix A.1.

102 **Structural identifiability of representations** Ours is also the first work to make clear the dis-
 103 tinction between such model-specific identifiability results and **structural identifiability** results such
 104 as disentanglement. We **formalize** an assumption on the data-generating process that allows us to
 105 extend our key **statistical** identifiability result to **structural identifiability of encoder-decoder models**,
 106 and define and characterize a rich class of data-generating processes which meet this assumption.
 107 This result is similar to other works that aim to “invert the data-generating process” (Zimmermann
 108 et al., 2021; Reizinger et al., 2025b; Von Kügelgen et al., 2021), including work on the isometry

assumption (Horan et al., 2021), some of which uses a different, average-case notion of near-isometry to claim near-recovery of the true latents in a nonlinear ICA model (Buchholz & Schölkopf, 2024). These prior works are far from real-world practice, with only Reizinger et al. (2025b) presenting any results on a real model with real data, showing that linear concept decoding is possible via parametric instance discrimination in ImageNet-X, but lacking a clear disentanglement result. In stark contrast, we illustrate a practical application of our theory by showing that we can improve out-of-distribution generalization in a real-world biological foundation model for cell microscopy via disentanglement. Our work also differs from prior work on causal representation learning (see Yao et al. (2025)) in that our **structural identifiability** result is completely unsupervised, relying on inductive biases rather than supervision in the form of interventions.

3 STABILITY THEORY

We begin by providing a novel theory of the stability of neural representations, with an eye toward self-supervised models. All theorems are presented informally with important constants in the main text, with full theorem statements, lemmata, proofs, and model-specific treatments in Appendix A.3.

3.1 STATISTICAL NEAR-IDENTIFIABILITY

We consider a data distribution supported on an arbitrary space \mathcal{X} . A representation learning model can be fully characterized by its parameter space Θ , its loss function, and the deterministic mapping from parameters to representation functions. Concretely, for each $\theta \in \Theta$, let $\mathcal{L}_\theta : \mathcal{X} \rightarrow \mathbb{R}$ denote the corresponding loss function, and define the model as $\mathcal{M} = \{\mathcal{L}_\theta : \theta \in \Theta\}$. If some component of θ parameterizes a representation function $f_\theta : \mathcal{X} \rightarrow \mathbb{R}^D$, then identifiability theory in machine learning aims to characterize the properties of f_θ after training by minimizing $\mathbb{E}[\mathcal{L}_\theta(x)]$ yields a set of parameters θ .

Definition 1. Let $\mathbf{P}(x)$ denote some data distribution supported on \mathcal{X} . Consider a machine learning model $\mathcal{M} = \{\mathcal{L}_\theta : \theta \in \Theta\}$, and let $F : \theta \mapsto f_\theta$ be some deterministic transform of the model parameters yielding a representation function $f_\theta : \mathcal{X} \rightarrow \mathbb{R}^D$. Let $\mathcal{S} \subset \Theta$ be the **set of minimizers** of $\mathbb{E}_{x \sim \mathbf{P}(x)}[\mathcal{L}_\theta(x)]$. For some group \mathcal{H} of functions from \mathbb{R}^D to itself, we say that $(\mathbf{P}, \mathcal{M}, F)$ is **statistically ϵ -nearly identifiable in expectation up to \mathcal{H}** if for every $\theta, \theta' \in \mathcal{S}$, we have $\|f_\theta - h \circ f_{\theta'}\| \leq \epsilon$ for some $h \in \mathcal{H}$.

Remark. For the remainder of this paper, we will use the the L^∞ norm (essential supremum with respect to \mathbf{P}) for functions taking values in the Euclidean space \mathbb{R}^D **endowed with the ℓ_2 norm**. When $\epsilon = 0$, we drop the ϵ -nearly and refer to the triple simply as **statistically identifiable in expectation up to \mathcal{H}** . When the identifiability is pointwise, we refer to the triple as **statistically identifiable in expectation**.

Intuition. This generalizes prior definitions of representation identifiability by the introduction of the “slack” term ϵ . Definition 1 says that a model’s representations as given by independent retrainings f_θ and $f_{\theta'}$ are near-identifiable if they are the same up to a simple transformation group \mathcal{H} (e.g. rotations) and a small amount of distortion ϵ . **In this way, we also generalize the classical definition of identifiability from mathematical statistics (Casella & Berger, 2001), see Appendix A.1 for a history.**

In this paper, we will mainly deal with near-identifiability of latent representations up to the function classes $\mathcal{H}_{\text{linear}}$, $\mathcal{H}_{\text{rigid}}$ and \mathcal{H}_σ . $\mathcal{H}_{\text{linear}}$ is the group of invertible linear transformations on \mathbb{R}^D , while $\mathcal{H}_{\text{rigid}}$ is the class of rigid linear transformations on \mathbb{R}^D , which consists of compositions of rotations, reflections and translations ($\mathcal{H}_{\text{rigid}} \subset \mathcal{H}_{\text{linear}}$). In practice, translations can be ignored by assuming e.g. zero mean of the representation distribution. Similarly, reflections only flip signs, and can usually also be ignored. It is therefore useful to imagine the main indeterminacy of $\mathcal{H}_{\text{rigid}}$ as being a special orthogonal matrix in $\mathbb{SO}(D)$, i.e. a rotation. \mathcal{H}_σ is the class of signed permutations of \mathbb{R}^D , which are generally not resolvable because there is no reasonable way to specify an ordering to the latent variables or signs to individual latent variables (should the x coordinate of an object in a scene be represented left-to-right, or right-to-left?).

Connection with prior results Existing representation identifiability results can easily be recast in our framework. For example, contrastive learning models using the InfoNCE loss with augmentation

162 distributions satisfying a particular isotropy condition in latent space are identifiable up to $\mathcal{H}_{\text{rigid}}$
 163 (Zimmermann et al., 2021). This isotropy condition is impossible to validate in practice without
 164 access to the ground-truth data-generating factors, reflecting the fact that it is a strong assumption on
 165 the true data-generating process.

166 Another result is due to Roeder et al. (2021), which applies to models whose losses take the following
 167 form and can be interpreted as exponential family negative log-likelihoods:
 168

$$\mathcal{L}_\theta(x, y) = -\eta_\theta(x)^\top \mathbf{t}_\theta(y) + A_\theta(x) = -\log q_\theta(y | x) \quad (1)$$

171 where q_θ is the approximating distribution, \mathbf{t}_θ is a sufficient statistics function, η_θ is the natural
 172 parameter function, and A_θ is the log partition function. As an example, \mathbf{t}_θ might map categorical
 173 labels to their corresponding vectors in a final linear weights matrix (covering the case of supervised
 174 multi-class classification, including next-token prediction). η_θ maps inputs to their representations,
 175 which are shown to be identifiable up to $\mathcal{H}_{\text{linear}}$ when pointwise equality of the losses is attained.
 176 In a short proof in Appendix A.3.1, we show that a simple sufficient richness condition on the
 177 approximating class extends this result to our definition of identifiable in expectation. Put together,
 178 this result means that “perfect optimization” on infinite data will yield a supervised or GPT-class
 179 model with the same penultimate-layer representations every time, up to some unknown linear
 180 transformation. **An extension of this result provides for the same kind of identifiability on a linear**
 181 **subspace of the representation space, allowing for the case of models with representations of different**
 182 **ambient dimension (Marconato et al., 2025). Nielsen et al. (2025) provides for a further generalization,**
 183 **deriving a notion of distance on the space of modeled likelihoods $\mathcal{Q} = \{q_\theta(y | x) : \theta \in \Theta\}$ such that**
 184 **closeness in distribution implies closeness in the penultimate-layer representations given by η_θ , a**
 185 **form of near-identifiability (see also Appendix A.3.1).**

186 Even these GPT results are limited because they only treat these penultimate-layer representations
 187 given by η , which are mapped *linearly* to the loss. For many models, we’re interested in repre-
 188 sentations from earlier layers which are mapped to the loss *nonlinearly*, such as with a nonlinear
 189 decoder or head. Our key result, captured in the following theorem, provides near-identifiability up
 190 to rigid transformations in such cases. The level of nearness ϵ is governed by the degree of local
 191 bi-Lipschitzness of this nonlinear mapping. This result allows us to treat earlier-layer representations
 192 in GPT or supervised classification models, for example, or the latent representations of (masked)
 193 autoencoders.

194 **Theorem 1. (Informal)** *Let $\mathbf{P}(x)$ be a data distribution, and let \mathcal{M} be a model with a parameter
 195 space Θ . Let $F : \theta \mapsto f_\theta$, $G : \theta \mapsto g_\theta$ and $H : \theta \mapsto g_\theta \circ f_\theta$. Then, if $(\mathbf{P}, \mathcal{M}, F)$ is statistically
 196 identifiable in expectation, then $(\mathbf{P}, \mathcal{M}, H)$ is statistically ϵ -nearly identifiable in expectation up to
 197 $\mathcal{H}_{\text{rigid}}$ for $\epsilon = c_D \sqrt{2L + L^2} \Delta$ where $1 + L$ is a local bi-Lipschitz constant bound for g_θ , and c_D and
 198 Δ are constants independent of the model (and L).*

199 **Intuition.** Here, we give the first general-purpose identifiability result for the internal representations
 200 (i.e. arbitrary-layer) of a broad class of models, including (masked) autoencoders, next-token
 201 predictors, and supervised learners. H parameterizes the end-to-end neural network $g_\theta \circ f_\theta$, which
 202 is assumed to have identifiable outputs: for example, when the loss is the mean squared error, the
 203 neural network learns the optimal function, namely the conditional mean. The identifiability of the
 204 internal representations given by f_θ (the “encoder”) is then governed by the local bi-Lipschitzness of
 205 the function g_θ (the “decoder”) mapping them to these identified outputs. **The bi-Lipschitz constraint**
 206 **controls the degree to which g_θ deforms distances. Intuitively, a bound on the local bi-Lipschitz**
 207 **constant is small when small changes in the latent variables result in small changes in the outputs of**
 208 **the network.** The proof is given in Appendix A.3.2, and we provide concrete examples for a number
 209 of architectures, including masked autoencoders, supervised learners, and GPTs in Appendices A.3.3
 210 and A.3.4.

211 This result is the most general we are aware of for quantifying representation identifiability. The local
 212 bi-Lipschitz condition is difficult to test empirically, but prior work has shown that many popular
 213 regularization techniques push neural networks toward a state of “dynamical isometry”, which can be
 214 viewed as a bi-Lipschitz condition (Xiao et al., 2018; Bachlechner et al., 2020; Miyato et al., 2018;
 215 Karras et al., 2020; Zhang et al., 2019) due to the singular values of the Jacobian concentrating near
 one. We derive the precise relationship in Appendix A.4.

216 3.2 RESOLVING LINEAR INDETERMINACIES WITH ICA
217

218 Later, we will illustrate applications of the near-identifiability result Theorem 1 to both vanilla
219 autoencoders and masked autoencoders. To do this, we will find it useful to resolve the remaining
220 linear indeterminacy in the latent space posed by $\mathcal{H}_{\text{linear}}$ or $\mathcal{H}_{\text{rigid}}$. We propose to do this by applying
221 independent components analysis to the latent representations. We do not provide any novel ICA
222 identifiability results in this work. Rather, we show that our conception of ϵ -nearness in identifiability
223 poses no further complications for the downstream application of ICA.

224 **Theorem 2.** *(Informal) Suppose $(\mathbf{P}, \mathcal{M}, F)$ is statistically ϵ -nearly identifiable up to $\mathcal{H}_{\text{linear}}$ for
225 $F : \theta \mapsto f_\theta$. Then, for a new model \mathcal{M}' which applies whitening and contrast function-based
226 independent components analysis to the latent representations given by f_θ and $F' : \theta \mapsto f'_\theta$ which
227 yields the transformed representations, $(\mathbf{P}, \mathcal{M}', F')$ is statistically ϵ' -near-identifiable up to \mathcal{H}_σ
228 for $\epsilon' = K\epsilon + K'\epsilon^2$, where K and K' are constants free of ϵ that depend on the spectrum of the
229 covariance matrix of the representations and the properties of the ICA contrast function.*

230 **Intuition.** Consider some representations in a model which are linearly identifiable, such as the
231 penultimate layer of a GPT-class model or the latent tokens of a masked autoencoder covered by
232 Theorem 1. Whitening reduces the linear indeterminacy to a rigid one, while ICA (if sufficiently well-
233 converged) resolves the final rigid indeterminacy to a signed permutation, with nearness preserved
234 (up to new constants) along each step.

235 3.3 FROM STATISTICAL TO STRUCTURAL IDENTIFIABILITY
236

238 While statistical identifiability on its own may be a useful property for reliability and analysis, there
239 has been recent interest in structural identifiability of representations, or the ability of the model to
240 recover some latent component of the data-generating process which is useful for some downstream
241 tasks. Below, we formalize the distinction between the two.

242 **Definition 2.** *Let $\mathbf{P}(u)$ denote a distribution over some unobservable parameters with support
243 $\mathcal{U} \subseteq \mathbb{R}^D$. Let $\mathbf{P}(x | u)$ denote some conditional distribution such that $u(x) = \arg \sup_{u \in \mathcal{U}} \mathbf{P}(x | u)$
244 is well-defined almost everywhere with respect to $\mathbf{P}(x)$, where $\mathbf{P}(x) = \int \mathbf{P}(x | u) \mathbf{P}(u) du$ is the
245 marginal distribution of the data with support \mathcal{X} . Consider a machine learning model $\mathcal{M} = \{\mathcal{L}_\theta : \theta \in$
246 $\Theta\}$, with solutions $\mathcal{S} \subset \Theta$ to the minimization of $\mathbb{E}_{x \sim \mathbf{P}(x)} [\mathcal{L}_\theta(x)]$. Let $F : \theta \mapsto f_\theta$ be a deterministic
247 transform of the parameters yielding a representation function $f_\theta : \mathcal{X} \rightarrow \mathbb{R}^D$. For some group of
248 functions \mathcal{H} from \mathbb{R}^D to itself, we say that $(\mathbf{P}, \mathcal{M}, F)$ ϵ -nearly identifies the structure u up to \mathcal{H} if
249 for all $\theta \in \mathcal{S}$, we have that f_θ satisfies $\|h \circ f_\theta - u\| \leq \epsilon$ for some $h \in \mathcal{H}$.*

250 **Intuition.** Statistical identifiability is in some sense *weaker* than structural identifiability. Statistical
251 identifiability is the condition that the representations are consistent, while structural identifiability
252 is the condition that the representations are consistently “correct”. In order to define utility, or
253 correctness, we need to assume the existence of some latent component of the data-generating process
254 that we’re aiming to recover, u . The well-studied setting of disentanglement (Locatello et al., 2019)
255 represents a special case where $\mathbf{P}(u)$ is assumed to have independent components. As an example,
256 in Section 4.4, we consider the situation where $\mathbf{P}(u)$ is a distribution over natural latent biological
257 factors along with independent technical variates, and x is generated via a smooth function of u
258 with smooth inverse, leaving $u(x)$ well-defined. In Appendix A.5, we provide a simple proof that
259 structural identifiability implies structural identifiability, including in the ϵ -near case provided that \mathcal{H}
260 is bounded in the sense of an operator norm.

261 Finally, we make precise the assumptions on the data-generating process necessary to extend our
262 statistical identifiability result in Theorem 2 to structural identifiability. We show that bi-Lipschitz
263 data-generating processes are structurally identified by reconstructing encoder-decoder models which
264 are nearly identifiable up to $\mathcal{H}_{\text{rigid}}$ in the sense of Theorem 1, and up to \mathcal{H}_σ when combined with ICA
265 as in Theorem 2. This is partly a generalization of an earlier result by Horan et al. (2021), which
266 covers the perfectly identifiable case.

267 **Theorem 3.** *(Informal) Let $\mathbf{P}(u)$ be some multivariate non-Gaussian distribution with independent
268 components and consider data $\mathbf{P}(x)$ generated by pushforward through a smooth diffeomorphism
269 g such that g is $(1 + \delta)$ -bi-Lipschitz. Let \mathcal{M} be a model with a sufficiently rich parameter space
270 Θ . Let $F : \theta \mapsto f_\theta$, $G : \theta \mapsto g_\theta$ and $H : \theta \mapsto g_\theta \circ f_\theta$. Then, if $(\mathbf{P}, \mathcal{M}, H)$ structurally identifies*

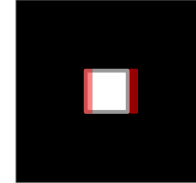
270 the identity function in expectation (i.e. attains perfect reconstruction), we have that $(\mathbf{P}, \mathcal{M}, F)$
 271 ϵ -nearly identifies the structure g^{-1} up to $\mathcal{H}_{\text{rigid}}$, and furthermore that a new model \mathcal{M}' which applies
 272 whitening and independent components analysis to the latent representations given by f_θ ϵ' -nearly
 273 identifies the structure g^{-1} up to \mathcal{H}_σ where ϵ and ϵ' depend on δ and Lipschitz bounds on g_θ , and
 274 ϵ' depends additionally on the spectrum of the covariance matrix of the representations and the
 275 properties of the ICA contrast function employed.

276
 277 **Intuition.** Structural identifiability is *stronger* than identifiability, so we require additional as-
 278 sumptions on the data-generating process to achieve it. In particular, here we assume that the
 279 data-generating function mapping “true” latents to observables is locally bi-Lipschitz, which com-
 280 bined with independence and non-Gaussianity is sufficient to nearly recover the true latents via ICA
 281 for any nearly identifiable reconstructing model with a locally bi-Lipschitz decoder. The proof is
 282 given in Appendix A.3.6.

283 3.3.1 BI-LIPSCHITZ DATA-GENERATING PROCESSES

284 Naturally, it’s useful to characterize what kinds of data-generating processes might be covered by
 285 Theorem 3. Several interesting image data-generating processes are known to approximately satisfy
 286 a Euclidean isometry condition (which is equivalent to a local 1-bi-Lipschitz constraint for smooth
 287 mappings) such as smooth articulations of cartoon faces (Tenenbaum et al., 2000; Horan et al.,
 288 2021). Furthermore, the success of regularization techniques similar to isometry constraints in diverse
 289 classes of neural network models in real-world settings suggests it is a useful inductive bias in
 290 practice as well (Karras et al., 2020; Lee et al., 2022). In the rest of this section, we aim to better
 291 characterize what these assumptions mean. Specifically, we give some examples of nearly isometric
 292 data-generating processes inspired by the popular `dSprites` dataset (Matthey et al., 2017) and show
 293 that disentanglement in this setting implies the structural identification of the true data-generating
 294 factors, using a technique developed by Grimes (2003).

295
 296 **Example** Consider a continuous relaxation of images, where a square black-
 297 and-white image is represented by an L^2 function $\iota : [-1, 1] \times [-1, 1] \rightarrow \{0, 1\}$, with $\iota(x, y)$ giving the value of the (x, y) th “pixel”. As an example,
 298 the image of a white square with radius $0 < r < 1$ in the centre of the “frame”
 299 is given by $\iota(x, y) = \mathbb{I}[|x| \leq r, |y| \leq r]$ where \mathbb{I} is the indicator function.
 300 One can first imagine a manifold of such images where the centre $p \in [a, b]$
 301 of the square is moved from left to right. We write this as a continuum of
 302 images produced by the smooth function $f : [a, b] \rightarrow L^2$ where $a + 1 \geq r$ and
 303 $1 - b \geq r$ to ensure that the square does not leave the frame. In this case, each
 304 “image” on the continuum $f(p)$ is the function $(x, y) \mapsto \mathbb{I}[|x - p| \leq r, |y| \leq r]$,
 305 where p is the square’s x coordinate.



306 Figure 1: A sim-
 307 ple isometric data-
 308 generating process.

309 We’ll show that f is a local isometry, meaning that it preserves a notion of distance perfectly. This is
 310 equivalent to a 1-bi-Lipschitz constraint. To see this, consider the Gateaux derivative of f , which is
 311 just the limiting behaviour of articulating the square ϵ units to the right:

$$312 f'(p) = \lim_{\epsilon \rightarrow 0} \frac{f(p + \epsilon) - f(p)}{\epsilon} \\ 313 = \lim_{\epsilon \rightarrow 0} \frac{1}{\epsilon} \left[\underbrace{\mathbb{I}[p + r < x < p + r + \epsilon, |y| < r]}_{\text{“gained” white pixels}} - \underbrace{\mathbb{I}[p - r - \epsilon < x < p - r, |y| < r]}_{\text{“lost” white pixels}} \right]$$

314 where the indicators in the limit represent the pixels that change when articulating the square ϵ units
 315 to the right. **Intuitively, shifting the square ϵ units to the right only changes ϵr pixels to the right (flips
 316 them from black to white) and ϵr pixels to the left (flips them from white to black) of the original
 317 square. The situation is drawn in Figure 1, where the white square has a gray border for clarity
 318 and the red shaded areas show the white pixels which are gained and lost by shifting the square ϵ units to
 319 the right. The isometry condition considers the situation as $\epsilon \rightarrow 0$ (intuitively, as the width of the red
 320 rectangles shrinks to zero).**

324 By an argument made formal in Appendix A.6, we can rely on something like preservation of the L^2
 325 norm under limits to have $\|f'(p)\|^2 = 2r$, which is constant when r is fixed. In the univariate case,
 326 this is sufficient for f to locally preserve a notion of distance. In particular, for any two values of the
 327 latent p_0 and p_1 we have

$$328 \quad |p_1 - p_0| \propto \int_{p_0}^{p_1} \|f'(p)\|^2 dp = 2r|p_1 - p_0|$$

$$329$$

$$330$$

331 where the integral is the usual geodesic distance along the manifold of “images”. Due to the constant
 332 $2r$, some literature refers to these as scaled isometries (Lee et al., 2022). In practice, we can typically
 333 ignore the scaling constant.

334 While sprites datasets are known to be overly simplistic, this analysis provides some intuition that
 335 interesting real-world image manifolds might usefully be approximated by isometries, or functions
 336 that are *nearly* isometries. For example, a similar analysis we defer to Appendix A.6 is illuminating
 337 for the multivariate case where both the radius r of the square and its x -coordinate p are varied. In this
 338 setting, we have that the Gateaux derivative is non-constant in r (specifically, the map is conformal).
 339 However, if we assume a compact support for the latents, i.e. that $p \in [a, b]$ and $r \in (0, R]$, the
 340 data-generating process is additionally B -bi-Lipschitz with the constant B dependent on a and b , and
 341 Theorem 3 applies.

342 4 EXPERIMENTS

343 We perform **four** sets of experiments: **direct validation of Theorem 1 on MNIST using vanilla**
 344 **autoencoders** (Section 4.1), direct validation of Theorems 1 and 2 in off-the-shelf pretrained **self-**
 345 **supervised learning** models (Section 4.2), an application of Theorem 3 to a classic disentanglement
 346 problem in several synthetic datasets (Section 4.3), and a real-world application to deconfounding for
 347 out-of-distribution generalization in a real-world foundation model for cell microscopy in biology
 348 (Section 4.4).

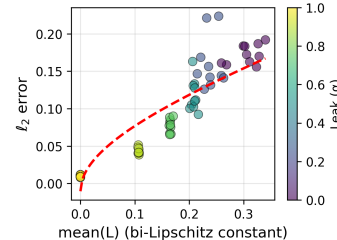
351 4.1 WARMUP: CONTROLLING IDENTIFIABILITY

352 We begin with experiments in a regime where the local bi-
 353 Lipschitz constant can be controlled as directly as possible,
 354 and examine whether our theory correctly predicts the level
 355 ϵ of near-identifiability. We consider fully-connected autoen-
 356 coders with 3-layer encoders and decoders, and orthogonal
 357 linear layers with LeakyReLU activations (with leak parameter
 358 $\alpha \in [0, 1]$). The local bi-Lipschitz constant of the decoders is
 359 therefore bounded by $1/\alpha^K$ where $K = 3$ is the number of
 360 layers in the decoder. For $\alpha = 1$, the network is linear, while for
 361 $\alpha = 0$, it’s a ReLU network. We fit pairs of autoencoders with
 362 different initializations and seeds to MNIST (LeCun & Cortes,
 363 2010), and assess the relationship between reconstruction error,
 364 empirical near-identifiability, and empirical measurements of
 365 the local bi-Lipschitz constant, which is manipulated by vary-
 366 ing α between 0 and 1. According to the proportionality in Theorem 1, we estimate how well
 367 the empirically estimated bi-Lipschitz term $\sqrt{L + L^2}$ predicts identifiability, as measured by the
 368 average ℓ_2 error from the optimal rigid transformation between the pair of latent spaces. Results are
 369 summarized in Figure 2. Full experimental details are available in Appendix A.7.1.

370 4.2 MEASURING IDENTIFIABILITY OF PRE-TRAINED MODELS

371 Our **next** aim is to validate the statistical near-identifiability up to linear (for GPT-class models,
 372 Theorem 1 of Roeder et al. (2021)) and rigid (for autoencoder-class and supervised models, Theorem
 373 1) transformations predicted by theory, and the ability of ICA to resolve the remaining linear
 374 indeterminacy (Theorem 2).

375 Matching our theory, we examine pairs of models that have the same architecture, loss, and are
 376 trained on the same dataset independently. Rigid similarities (rigid transforms with a scaling constant



377 Figure 2: Controlling the bi-
 378 Lipschitz constant L leads to im-
 379 proved identifiability (reduced ℓ_2
 380 error).

378 to allow for varying regularization across model pairs), linear transformations and ICA transforms are
 379 estimated between representation spaces. We measure near-identifiability with the average ℓ_2 error in
 380 the self-supervised model’s representation space, along with the efficiency of the ICA transform as
 381 the percentage reduction of ℓ_2 error relative to the rigid transform (since the degrees of freedom are
 382 roughly the same). Results are shown in Table 1.

383 GPT-class models exhibit ex-
 384 cellent linear alignment, as
 385 predicted by the theory of
 386 Roeder et al. (2021). As pre-
 387 dicted by our theory, MAEs
 388 exhibit rigid alignment up to a
 389 similar level of error, notably
 390 including one example across
 391 model sizes. In all cases, ICA
 392 mitigates a substantial portion
 393 of the indeterminacy due to
 394 the linear variation, notably
 395 without any supervision. In
 396 particular, for MAE models,
 397 ICA is nearly 60% as efficient as computing the optimal rigid transform between the two models in a
 398 fully-supervised fashion. Full experimental details are available in Appendix A.7.2.

Model Pair	Permutation	Supervised		ICA (% eff.)
		Rigid	Linear	
Pythia-160M-0 → Pythia-160M-1	0.219	0.150	0.131	0.202 (25%)
MAE-timm → MAE-original	0.197	0.109	0.036	0.145 (59%)
CheXpert-small → CheXpert-base	0.218	0.104	0.048	0.175 (38%)
ResNet-18-fc-1 → ResNet-18-fc-2	0.382	0.206	0.175	0.312 (40%)

Table 1: **Supervised and unsupervised alignment scores between pairs of models which measure empirical identifiability.** The optimal transforms (permutation, rigid, linear, or ICA) are estimated between the two models, and average ℓ_2 errors normalized by latent diameter are reported. For ICA, we also report its efficiency as the reduction of ℓ_2 error from the permutation to the rigid transform.

4.3 DISENTANGLEMENT USING VANILLA AUTOENCODERS

401 Next, we assess whether our theory correctly predicts **structural identifiability** of the ground-truth
 402 data-generating factors in synthetic datasets matching the assumptions of Theorem 3. We examine
 403 vanilla autoencoders, an appealing architecture due to their simplicity. In such simple models, weight
 404 decay is known to be sufficient to regularize the Lipschitz constant of the decoder, thus making it a
 405 good testbed for our theory (Zhang et al., 2019).

406 We use a well-established experimental testbed for assessing unsupervised disentanglement, specifi-
 407 cally following the exact experimental protocol from Hsu et al. (2023). As baselines, we include a
 408 β -VAE (Higgins et al., 2017), β -total correlation VAE (Chen et al., 2018), and BioAE (Whittington
 409 et al., 2023), all of which leverage specialized regularization to achieve disentanglement. For compari-
 410 son, we follow the supervised model selection strategy of Hsu et al. (2023), which shows best-case
 411 performance (Locatello et al., 2020).

412 For each dataset, we train a vanilla autoencoder with the only hyperparameter we vary being weight
 413 decay. Then, ICA is applied to its latent space. Models are evaluated on four datasets. Shapes3D is
 414 a toyish sprites dataset (Hsu et al., 2023; Burgess & Kim, 2018). Falcor3D and Isaac3D consist of
 415 rendered images of a living room and kitchen, respectively (Nie et al., 2020). MPI3D consists of real
 416 images of a real-world robotics setup (Gondal et al., 2019). Disentanglement of the learned latents is
 417 evaluated according to InfoMEC (Hsu et al., 2023) which consists of three complementary metrics:
 418 modularity (the degree to which each learned latent encodes only one true source), explicitness (the
 419 degree to which the latents capture all information about a source), and less important, compactness
 420 (the degree to which each source is encoded in only one latent). InfoMEC aims to resolve many of
 421

422 Table 2: Disentanglement metrics (*InfoM*, *InfoE*, *InfoC*), of which *InfoM* and *InfoE* are the most
 423 important. AE + ICA performs comparably to some of the best disentanglement-specific neural
 424 networks, with almost no tuning. Results marked with (*) are quoted without reproduction from Hsu
 425 et al. (2023). Bolded metrics have the highest point estimates. Full details in Appendix A.7.3.

model	aggregated	Shapes3D			MPI3D			Falcor3D			Isaac3D		
		<i>InfoM</i>	<i>InfoE</i>	<i>InfoC</i>	<i>InfoM</i>	<i>InfoE</i>	<i>InfoC</i>	<i>InfoM</i>	<i>InfoE</i>	<i>InfoC</i>	<i>InfoM</i>	<i>InfoE</i>	<i>InfoC</i>
AE	(0.39 0.76 0.25)	(0.34 0.99 0.16)	(0.42 0.40 0.31)	(0.37 0.83 0.20)	(0.41 0.80 0.34)								
β -VAE*	(0.59 0.81 0.55)	(0.59 0.99 0.49)	(0.45 0.71 0.51)	(0.71 0.73 0.70)	(0.60 0.80 0.51)								
β -TCVAE*	(0.58 0.72 0.59)	(0.61 0.82 0.62)	(0.51 0.60 0.57)	(0.66 0.74 0.71)	(0.54 0.70 0.46)								
BioAE*	(0.54 0.75 0.36)	(0.56 0.98 0.44)	(0.45 0.66 0.36)	(0.54 0.73 0.31)	(0.63 0.65 0.33)								
AE + ICA (ours)	(0.65 0.83 0.40)	(0.79 0.99 0.52)	(0.44 0.66 0.31)	(0.71 0.83 0.33)	(0.64 0.82 0.43)								

432 the issues with the DCI framework of disentanglement evaluations, including removing the need to
 433 select hyperparameters which can affect results (Hsu et al., 2023).
 434

435 Vanilla autoencoders with ICA in latent space outperform specialized disentanglement models most
 436 of the time (Table 2), and on average perform better than all. Experimental runtime is roughly 6 hours
 437 per autoencoder hyperparameter setting on a single GPU (roughly 720 GPU hours total).
 438

439 4.4 DECONFOUNDING AT FOUNDATION MODEL-SCALE

440 High-throughput screens have become a critical tool in modern biology, particularly for drug discovery
 441 (Chandrasekaran et al., 2023). One example of such screenings is cell painting (Chandrasekaran
 442 et al., 2023; Sypetkowski et al., 2023), where a perturbation is applied (or not) to a collection of cells,
 443 which are then stained and imaged. A key challenge in the application of machine learning to these
 444 data is the presence of complex technical variation (“batch effects”) that is not biologically significant
 445 (Arevalo et al., 2024; Chandrasekaran et al., 2023; Lin & Lu, 2022; Sypetkowski et al., 2023; Ando
 446 et al., 2017). For example, data collected from different microscopes, labs, or even just in different
 447 experiments can exhibit variation that is not of interest to the practitioner, potentially confounding
 448 results. A fundamental task in this setting is to quantify the degree to which a perturbation has a
 449 significant effect, which is challenging given that we have access only to high-dimensional, noisy
 450 observations in the form of images confounded by batch effects (Bereket & Karaletsos, 2023). In
 451 particular, we almost never have the ability to measure all sources of batch variation, and so it is of
 452 specific interest to be able to disentangle technical from biological variation without supervision.
 453

454 We explore an application of Theorem 3 by applying independent component analysis to the latent
 455 space of OpenPhenom (Kraus et al., 2024), a large, open masked autoencoder trained on Rxrx3-core, a
 456 large library of cell painting images (Kraus et al., 2025). Downstream, we consider the task where the
 457 inferred embeddings are used to predict whether a given perturbation has been applied (i.e. classify
 458 “control” vs. “perturbed”). Because we are primarily interested in whether the procedure enhances
 459 out-of-distribution generalization, we consider downstream classifiers trained on a subset of batches
 460 and evaluated on a held-out subset of batches.

461 **Inference & evaluation** We perform inference on all images from Rxrx3-core and estimate the
 462 whitening and independent components analysis models at the patch level by randomly subsampling
 463 a patch from each image. We consider four conditions: the original embedding (Base), the embedding
 464 whitened with principal components analysis (PCA), the whitened embedding rotated using ICA
 465 (PCA + ICA), and as a baseline, the whitened embedding rotated randomly (PCA + Rand). Plates are
 466 used as the batch indicator, while a single patch-level embedding is used for each image. For each
 467 embedding condition (raw, whitened, whitened + ICA, whitened + random rotation), we hold out 20%
 468 of plates and train a gradient boosting classifier (Ke et al., 2017) on the remaining 80% of plates in a
 469 k -fold cross-validation scheme. Because some plates do not contain any perturbed samples (i.e. are
 470 entirely controls), we ensure that this split is roughly stratified on the label (“perturbed” vs. “control”).
 471 Perturbation classification is evaluated by the area under the receiver operator characteristic curve
 472 (AUROC). Embedding inference took approximately 1 hour on a single GPU, while ICA estimation
 473 took about 1 hour on 128 CPU cores with 128 GB RAM.
 474

475 Table 3: Results from a downstream perturbation classification task. Each row represents a gene
 476 consisting of (#) separate experiments with different CRISPR guides. All experiments use the same
 477 set of 22,062 controls. Base = untransformed embeddings, PCA = whitened embeddings, PCA +
 478 ICA = whitened embeddings with ICA rotation applied, PCA + Rand = whitened embeddings with a
 479 random rotation applied.

480 Gene	481 Mean AUROC (\uparrow)				482 Sparsity (\uparrow more sparse)			
	483 Base	484 PCA	485 PCA + ICA	486 PCA + Rand	487 Base	488 PCA	489 PCA + ICA	490 PCA + Rand
CYP11B1 (1)	0.663	0.692	0.709	0.678	0.184	0.204	0.237	0.188
EIF3H (1)	0.682	0.724	0.749	0.725	0.192	0.224	0.268	0.214
HCK (1)	0.670	0.693	0.711	0.668	0.156	0.208	0.241	0.166
MTOR (6)	0.663	0.690	0.705	0.679	0.166	0.201	0.233	0.186
PLK1 (6)	0.803	0.811	0.815	0.792	0.251	0.307	0.305	0.262
SRC (1)	0.660	0.694	0.706	0.676	0.170	0.214	0.240	0.184

486 **Results** Whitening alone often enhances the performance of downstream classification from the
 487 embeddings. The application of ICA consistently improves the performance even further (Table 3).
 488 To understand the source of the improvement, we measure sparsity with a measure called Hoyer
 489 sparsity which characterizes how biased trees are toward selecting a particular subset of features
 490 (Hoyer, 2004) defined as $\text{Sparsity}[\mathbf{c}] = \frac{\sqrt{D} - \frac{1}{\|\mathbf{c}\|_2}}{\sqrt{D-1}}$ for a D -dimensional vector of split fractions \mathbf{c}
 491 such that $\|\mathbf{c}\|_1 = 1$ and where c_d measures the fraction of times the d th variable was used in a split
 492 (higher \rightarrow more important). The sparsity score is zero when all features are used equally often.
 493 Sparsity increases markedly with both whitening and ICA.
 494

495 However, this measure does not specifically show that the information
 496 being ignored as a result of the increased sparsity specifically
 497 has to do with the distinction between technical and biological
 498 variation. To assess this, we measure how well the information
 499 useful for predicting the biological effect is concentrated in the
 500 top $k\%$ of predictors. Denote by $\mathbf{z}_{k\%}$ the top $k\%$ most important
 501 features for the prediction of the biological effect y of interest, and
 502 by $\mathbf{z}'_{k\%}$ the remaining features. Then, the concentration is given
 503 by $\text{Concentration}[y] = \frac{\text{AUROC}[y:\mathbf{z}_{k\%}]}{\text{AUROC}[y:\mathbf{z}'_{k\%}]} - 1$, i.e., the improvement in
 504 predicting perturbation y from the top features versus the bottom.
 505 The concentration increases uniformly with whitening and with ICA (Table 4.4), even in the case of
 506 PLK1 guides where it does not confer a substantial gain in out-of-distribution AUROC. The results
 507 are not sensitive to reasonable values of k (Appendix A.7.4). Interestingly, the results suggest that
 508 whitening alone biases the representation toward becoming axis-aligned even without ICA.
 509

5 DISCUSSION

510 We have developed a theory of statistical near-identifiability of neural representations which is
 511 applicable to the internal representations of real-world self-supervised models. Notably, in contrast
 512 to prior work, our result requires few assumptions on the data-generating process, instead trading
 513 these off for assumptions on the model alone, and applies to a broad class of models including
 514 supervised learners, next-token predictors, and self-supervised learners. Additionally, we have shown
 515 that additional assumptions on the data-generating process can confer an even stronger result: namely,
 516 provable structural identifiability of the latent variables which generated the observables. We directly
 517 test our theory in real-world, off-the-shelf, pretrained self-supervised models. Furthermore, we
 518 leverage our theory to motivate the application of ICA to the latent spaces of self-supervised models
 519 and show that it can achieve state-of-the-art disentanglement results, including some of the first
 520 disentanglement results for out-of-distribution generalization in real-world data.
 521

522 **Limitations & future work** The primary limitation of our work is the difficulty in empirically
 523 testing the bi-Lipschitz assumptions necessary for our theory. Instead, we test the downstream
 524 effects of our theory in four sets of experiments, and offer arguments from prior work which show
 525 that common regularization techniques which enable training of practical-scale neural networks
 526 (often referred to as “dynamical isometry”, see also Appendix A.4) may lead to this condition.
 527 Interestingly, because the local bi-Lipschitz assumption is largely agnostic to data modality and
 528 model implementation details, it potentially applies to a broad class of both data-generating processes
 529 and models. As such, it may be an interesting lens for studying the phenomenon of cross-model
 530 representation convergence (Maiorca et al., 2023; Fumero et al., 2024), which is largely unaddressed
 531 by existing theory because existing identifiability results each require different assumptions on the
 532 data-generating process for different models (Huh et al., 2024; Reizinger et al., 2025a). Although we
 533 echo the calls of Reizinger et al. (2025a) for extensions to the practical regime (e.g. finite samples,
 534 imperfect optimization), we do not treat this case here, although it could be an extension of our
 535 framework. Additionally, because ours are the first identifiability results that apply to the intermediate
 536 layers of transformer-based next-token predictors, they may be useful for the interpretation of these
 537 models (Basile et al., 2025). In particular, Liu et al. (2025) show that discrete concept models learned
 538 atop last-layer GPT representations render the entire model end-to-end linearly identifiable, and the
 539 results of our paper suggest that this technique may work for intermediate-layer representations as
 well.

Model	Concentration (\uparrow)
Base	0.163
PCA	0.332
PCA + ICA	0.386
PCA + Rand	0.287

Table 4: Concentration of biological variation in the top 25% of features.

540 REFERENCES

541
 542 P. Alestalo, D. A. Trotsenko, and J. Väisälä. Isometric approximation. *Israel Journal of Mathematics*,
 543 125(1):61–82, Dec 2001. ISSN 1565-8511. doi: 10.1007/BF02773375. URL <https://doi.org/10.1007/BF02773375>.

544
 545 D. Michael Ando, Cory Y. McLean, and Marc Berndl. Improving phenotypic measurements in
 546 high-content imaging screens. *bioRxiv*, 2017. doi: 10.1101/161422. URL <https://www.biorxiv.org/content/early/2017/07/10/161422>.

547
 548 John Arevalo, Ellen Su, Jessica D. Ewald, Robert van Dijk, Anne E. Carpenter, and Shantanu Singh.
 549 Evaluating batch correction methods for image-based cell profiling. *Nature Communications*,
 550 15(1):6516, Aug 2024. ISSN 2041-1723. doi: 10.1038/s41467-024-50613-5. URL <https://doi.org/10.1038/s41467-024-50613-5>.

551
 552 Thomas Bachlechner, Bodhisattwa Prasad Majumder, Huanru Henry Mao, Garrison W. Cottrell,
 553 and Julian McAuley. Rezero is all you need: Fast convergence at large depth, 2020. URL
 554 <https://arxiv.org/abs/2003.04887>.

555
 556 Alexei Baevski, Yuhao Zhou, Abdelrahman Mohamed, and Michael Auli. wav2vec 2.0:
 557 A framework for self-supervised learning of speech representations. In H. Larochelle,
 558 M. Ranzato, R. Hadsell, M.F. Balcan, and H. Lin (eds.), *Advances in Neural In-*
 559 *formation Processing Systems*, volume 33, pp. 12449–12460. Curran Associates, Inc.,
 560 2020. URL https://proceedings.neurips.cc/paper_files/paper/2020/file/92d1e1eb1cd6f9fba3227870bb6d7f07-Paper.pdf.

561
 562 Lorenzo Basile, Valentino Maiorca, Luca Bortolussi, Emanuele Rodolà, and Francesco Locatello.
 563 Residual transformer alignment with spectral decomposition, 2025. URL <https://arxiv.org/abs/2411.00246>.

564
 565 Michael Bereket and Theofanis Karaletsos. Modelling cellular perturbations with the
 566 sparse additive mechanism shift variational autoencoder. In A. Oh, T. Naumann,
 567 A. Globerson, K. Saenko, M. Hardt, and S. Levine (eds.), *Advances in Neu-*
 568 *ral Information Processing Systems*, volume 36, pp. 1–12. Curran Associates, Inc.,
 569 2023. URL https://proceedings.neurips.cc/paper_files/paper/2023/file/0001ca33ba34ce0351e4612b744b3936-Paper-Conference.pdf.

570
 571 Anthony Brohan, Noah Brown, Justice Carbajal, Yevgen Chebotar, Xi Chen, Krzysztof Choromanski,
 572 Tianli Ding, Danny Driess, Avinava Dubey, Chelsea Finn, Pete Florence, Chuyuan Fu, Montse Gon-
 573 zalez Arenas, Keerthana Gopalakrishnan, Kehang Han, Karol Hausman, Alex Herzog, Jasmine
 574 Hsu, Brian Ichter, Alex Irpan, Nikhil Joshi, Ryan Julian, Dmitry Kalashnikov, Yuheng Kuang,
 575 Isabel Leal, Lisa Lee, Tsang-Wei Edward Lee, Sergey Levine, Yao Lu, Henryk Michalewski,
 576 Igor Mordatch, Karl Pertsch, Kanishka Rao, Krista Reymann, Michael Ryoo, Grecia Salazar,
 577 Pannag Sanketi, Pierre Sermanet, Jaspair Singh, Anikait Singh, Radu Soricu, Huong Tran, Vincent
 578 Vanhoucke, Quan Vuong, Ayzaan Wahid, Stefan Welker, Paul Wohlhart, Jialin Wu, Fei Xia, Ted
 579 Xiao, Peng Xu, Sichun Xu, Tianhe Yu, and Brianna Zitkovich. Rt-2: Vision-language-action
 580 models transfer web knowledge to robotic control. In *arXiv preprint arXiv:2307.15818*, 2023.

581
 582 Simon Buchholz and Bernhard Schölkopf. Robustness of nonlinear representation learning. In Ruslan
 583 Salakhutdinov, Zico Kolter, Katherine Heller, Adrian Weller, Nuria Oliver, Jonathan Scarlett, and
 584 Felix Berkenkamp (eds.), *Proceedings of the 41st International Conference on Machine Learning*,
 585 volume 235 of *Proceedings of Machine Learning Research*, pp. 4785–4821. PMLR, 21–27 Jul
 2024. URL <https://proceedings.mlr.press/v235/buchholz24a.html>.

586
 587 Chris Burgess and Hyunjik Kim. 3d shapes dataset. <https://github.com/deepmind/3dshapes-dataset/>,
 2018.

588
 589 George Casella and Roger Berger. *Statistical Inference*. Duxbury Resource Center, June 2001. ISBN
 0534243126.

590
 591 Marc Castella, Selwa Rafi, Pierre Comon, and Wojciech Pieczynski. Separation of instantaneous
 592 mixtures of a particular set of dependent sources using classical ica methods. *EURASIP Journal*
 593 *on Advances in Signal Processing*, 2013(1):62, Mar 2013. ISSN 1687-6180. doi: 10.1186/1687-6180-2013-62. URL <https://doi.org/10.1186/1687-6180-2013-62>.

594 Srinivas Niranj Chandrasekaran, Jeanelle Ackerman, Eric Alix, D. Michael Ando, John Arevalo,
 595 Melissa Bennion, Nicolas Boisseau, Adriana Borowa, Justin D. Boyd, Laurent Brino, Patrick J.
 596 Byrne, Hugo Ceulemans, Carolyn Ch'ng, Beth A. Cimini, Djork-Arne Clevert, Nicole Deflaux,
 597 John G. Doench, Thierry Dorval, Regis Doyonnas, Vincenza Dragone, Ola Engkvist, Patrick W.
 598 Faloon, Briana Fritchman, Florian Fuchs, Sakshi Garg, Tamara J. Gilbert, David Glazer, David
 599 Gnutt, Amy Goodale, Jeremy Grignard, Judith Guenther, Yu Han, Zahra Hanifehlou, Santosh
 600 Hariharan, Desiree Hernandez, Shane R. Horman, Gisela Hormel, Michael Huntley, Ilknur Icke,
 601 Makiyo Iida, Christina B. Jacob, Steffen Jaensch, Jawahar Khetan, Maria Kost-Alimova, Tomasz
 602 Krawiec, Daniel Kuhn, Charles-Hugues Lardeau, Amanda Lembke, Francis Lin, Kevin D. Little,
 603 Kenneth R. Lofstrom, Sofia Lotfi, David J. Logan, Yi Luo, Franck Madoux, Paula A. Marin
 604 Zapata, Brittany A. Marion, Glynn Martin, Nicola Jane McCarthy, Lewis Mervin, Lisa Miller,
 605 Haseeb Mohamed, Tiziana Monteverde, Elizabeth Mouchet, Barbara Nicke, Arnaud Ogier, Anne-
 606 Laure Ong, Marc Osterland, Magdalena Otracka, Pieter J. Peeters, James Pilling, Stefan Prechtl,
 607 Chen Qian, Krzysztof Rataj, David E. Root, Sylvie K. Sakata, Simon Scrace, Hajime Shimizu,
 608 David Simon, Peter Sommer, Craig Spruill, Iffat Sumia, Susanne E. Swalley, Hiroki Terauchi,
 609 Ammandine Thibaudeau, Amy Unruh, Jelle Van de Waeter, Michiel Van Dyck, Carlo van Staden,
 610 Michał Warchał, Erin Weisbart, Amélie Weiss, Nicolas Wiest-Daessle, Guy Williams, Shan
 611 Yu, Bolek Zapiec, Marek Żyła, Shantanu Singh, and Anne E. Carpenter. JUMP Cell Painting
 612 dataset: morphological impact of 136,000 chemical and genetic perturbations, March 2023. URL
 613 <https://www.biorxiv.org/content/10.1101/2023.03.23.534023v2>. Pages:
 614 2023.03.23.534023 Section: New Results.

615 Ricky T. Q. Chen, Xuechen Li, Roger B Grosse, and David K Duvenaud. Isolating sources of disentan-
 616 glement in variational autoencoders. In S. Bengio, H. Wallach, H. Larochelle, K. Grauman, N. Cesa-
 617 Bianchi, and R. Garnett (eds.), *Advances in Neural Information Processing Systems*, volume 31.
 618 Curran Associates, Inc., 2018. URL https://proceedings.neurips.cc/paper_files/paper/2018/file/1ee3dfcd8a0645a25a35977997223d22-Paper.pdf.

619 Wenlin Chen, Julien Horwood, Juyeon Heo, and José Miguel Hernández-Lobato. Leveraging task
 620 structures for improved identifiability in neural network representations, 2024. URL <https://arxiv.org/abs/2306.14861>.

621 Pierre Comon. Independent component analysis, a new concept? *Signal Processing*, 36(3):287–314,
 622 1994. ISSN 0165-1684. doi: [https://doi.org/10.1016/0165-1684\(94\)90029-9](https://doi.org/10.1016/0165-1684(94)90029-9). URL <https://www.sciencedirect.com/science/article/pii/0165168494900299>. Higher
 623 Order Statistics.

624 Oswaldo de Oliveira. The implicit and the inverse function theorems: Easy proofs. *Real Analysis
 625 Exchange*, 39(1):207, 2014. ISSN 0147-1937. doi: 10.14321/realanalexch.39.1.0207. URL
 626 <http://dx.doi.org/10.14321/realanalexch.39.1.0207>.

627 Marco Fumero, Marco Pegoraro, Valentino Maiorca, Francesco Locatello, and Emanuele Rodolà.
 628 Latent functional maps: a spectral framework for representation alignment. In A. Globerson,
 629 L. Mackey, D. Belgrave, A. Fan, U. Paquet, J. Tomczak, and C. Zhang (eds.), *Ad-
 630 vances in Neural Information Processing Systems*, volume 37, pp. 66178–66203. Curran As-
 631 sociates, Inc., 2024. URL https://proceedings.neurips.cc/paper_files/paper/2024/file/79be41d858841037987964e3f5caf76d-Paper-Conference.pdf.

632 Muhammad Waleed Gondal, Manuel Wuthrich, Djordje Miladinovic, Francesco Locatello, Mar-
 633 tin Breidt, Valentin Volchkov, Joel Akpo, Olivier Bachem, Bernhard Schölkopf, and Stefan
 634 Bauer. On the transfer of inductive bias from simulation to the real world: a new disentan-
 635 glement dataset. In H. Wallach, H. Larochelle, A. Beygelzimer, F. d'Alché-Buc, E. Fox, and
 636 R. Garnett (eds.), *Advances in Neural Information Processing Systems*, volume 32. Curran As-
 637 sociates, Inc., 2019. URL <https://proceedings.neurips.cc/paper/2019/file/d97d404b6119214e4a7018391195240a-Paper.pdf>.

638 Carrie Grimes. *NEW METHODS IN NONLINEAR DIMENSIONALITY REDUCTION*. PhD thesis,
 639 05 2003.

640 Thomas Hayes, Roshan Rao, Halil Akin, Nicholas J. Sofroniew, Deniz Oktay, Zeming Lin, Robert
 641 Verkuil, Vincent Q. Tran, Jonathan Deaton, Marius Wiggert, Rohil Badkundri, Irhum Shafkat,

648 Jun Gong, Alexander Derry, Raul S. Molina, Neil Thomas, Yousuf A. Khan, Chetan Mishra,
 649 Carolyn Kim, Liam J. Bartie, Matthew Nemeth, Patrick D. Hsu, Tom Sercu, Salvatore Candido,
 650 and Alexander Rives. Simulating 500 million years of evolution with a language model. *Science*,
 651 387(6736):850–858, 2025. doi: 10.1126/science.ads0018. URL <https://www.science.org/doi/10.1126/science.ads0018>.

652

653 Irina Higgins, Loic Matthey, Arka Pal, Christopher Burgess, Xavier Glorot, Matthew Botvinick,
 654 Shakir Mohamed, and Alexander Lerchner. beta-VAE: Learning basic visual concepts with a
 655 constrained variational framework. In *International Conference on Learning Representations*,
 656 2017. URL <https://openreview.net/forum?id=Sy2fzU9gl>.

657

658 Daniella Horan, Eitan Richardson, and Yair Weiss. When is unsupervised disentanglement possi-
 659 ble? In M. Ranzato, A. Beygelzimer, Y. Dauphin, P.S. Liang, and J. Wortman Vaughan (eds.),
 660 *Advances in Neural Information Processing Systems*, volume 34, pp. 5150–5161. Curran Asso-
 661 ciates, Inc., 2021. URL https://proceedings.neurips.cc/paper_files/paper/2021/file/29586cb449c90e249f1f09a0a4ee245a-Paper.pdf.

662

663 Patrik O. Hoyer. Non-negative matrix factorization with sparseness constraints, 2004. URL <https://arxiv.org/abs/cs/0408058>.

664

665 Kyle Hsu, William Dorrell, James Whittington, Jiajun Wu, and Chelsea Finn. Disentanglement via la-
 666 tent quantization. In A. Oh, T. Naumann, A. Globerson, K. Saenko, M. Hardt, and S. Levine (eds.),
 667 *Advances in Neural Information Processing Systems*, volume 36, pp. 45463–45488. Curran Asso-
 668 ciates, Inc., 2023. URL https://proceedings.neurips.cc/paper_files/paper/2023/file/8e63972d4d9d81b31459d787466ce271-Paper-Conference.pdf.

669

670

671 Minyoung Huh, Brian Cheung, Tongzhou Wang, and Phillip Isola. Position: The platonic represen-
 672 tation hypothesis. In Ruslan Salakhutdinov, Zico Kolter, Katherine Heller, Adrian Weller, Nuria
 673 Oliver, Jonathan Scarlett, and Felix Berkenkamp (eds.), *Proceedings of the 41st International
 674 Conference on Machine Learning*, volume 235 of *Proceedings of Machine Learning Research*, pp.
 675 20617–20642. PMLR, 21–27 Jul 2024. URL <https://proceedings.mlr.press/v235/huh24a.html>.

676

677 A. Hyvärinen and E. Oja. Independent component analysis: algorithms and applica-
 678 tions. *Neural Networks*, 13(4):411–430, 2000. ISSN 0893-6080. doi: [https://doi.org/10.1016/S0893-6080\(00\)00026-5](https://doi.org/10.1016/S0893-6080(00)00026-5). URL <https://www.sciencedirect.com/science/article/pii/S0893608000000265>.

679

680

681 Tero Karras, Samuli Laine, Miika Aittala, Janne Hellsten, Jaakko Lehtinen, and Timo Aila. Analyzing
 682 and improving the image quality of stylegan. In *Proceedings of the IEEE/CVF Conference on
 683 Computer Vision and Pattern Recognition (CVPR)*, June 2020.

684

685 Guolin Ke, Qi Meng, Thomas Finley, Taifeng Wang, Wei Chen, Weidong Ma, Qiwei Ye, and Tie-Yan
 686 Liu. Lightgbm: a highly efficient gradient boosting decision tree. In *Proceedings of the 31st
 687 International Conference on Neural Information Processing Systems*, NIPS’17, pp. 3149–3157,
 688 Red Hook, NY, USA, 2017. Curran Associates Inc. ISBN 9781510860964.

689

690 Ilyes Khemakhem, Diederik P. Kingma, Ricardo Pio Monti, and Aapo Hyvärinen. Variational
 691 autoencoders and nonlinear ica: A unifying framework, 2020a. URL <https://arxiv.org/abs/1907.04809>.

692

693 Ilyes Khemakhem, Ricardo Pio Monti, Diederik P. Kingma, and Aapo Hyvärinen. Ice-beem:
 694 Identifiable conditional energy-based deep models based on nonlinear ica, 2020b. URL <https://arxiv.org/abs/2002.11537>.

695

696 Diederik P. Kingma and Jimmy Ba. Adam: A method for stochastic optimization. In Yoshua Bengio
 697 and Yann LeCun (eds.), *ICLR (Poster)*, 2015. URL <http://dblp.uni-trier.de/db/conf/iclr/iclr2015.html#KingmaB14>.

698

699

700 Max Klabunde, Tassilo Wald, Tobias Schumacher, Klaus Maier-Hein, Markus Strohmaier, and Florian
 701 Lemmerich. Resi: A comprehensive benchmark for representational similarity measures, 2025.
 URL <https://arxiv.org/abs/2408.00531>.

702 T. C. Koopmans and O. Reiersøl. The identification of structural characteristics. *The Annals of*
 703 *Mathematical Statistics*, 21(2):165–181, 1950. ISSN 00034851. URL <http://www.jstor.org/stable/2236899>.

704

705 Oren Kraus, Kian Kenyon-Dean, Saber Saberian, Maryam Fallah, Peter McLean, Jess Leung, Vasudev
 706 Sharma, Ayla Khan, Jia Balakrishnan, Safiye Celik, et al. Masked autoencoders for microscopy are
 707 scalable learners of cellular biology. In *Proceedings of the IEEE/CVF Conference on Computer*
 708 *Vision and Pattern Recognition*, pp. 11757–11768, 2024.

709

710 Oren Kraus, Federico Comitani, John Urbanik, Kian Kenyon-Dean, Lakshmanan Arumugam, Saber
 711 Saberian, Cas Wognum, Safiye Celik, and Imran S. Haque. Rxrx3-core: Benchmarking drug-
 712 target interactions in high-content microscopy, 2025. URL <https://arxiv.org/abs/2503.20158>.

713

714 Sebastien Lachapelle, Tristan Deleu, Divyat Mahajan, Ioannis Mitliagkas, Yoshua Bengio, Si-
 715 mon Lacoste-Julien, and Quentin Bertrand. Synergies between disentanglement and spar-
 716 sity: Generalization and identifiability in multi-task learning. In Andreas Krause, Emma
 717 Brunskill, Kyunghyun Cho, Barbara Engelhardt, Sivan Sabato, and Jonathan Scarlett (eds.),
 718 *Proceedings of the 40th International Conference on Machine Learning*, volume 202 of *Pro-
 719 ceedings of Machine Learning Research*, pp. 18171–18206. PMLR, 23–29 Jul 2023. URL
 720 <https://proceedings.mlr.press/v202/lachapelle23a.html>.

721

722 Yann LeCun and Corinna Cortes. MNIST handwritten digit database. 2010. URL <http://yann.lecun.com/exdb/mnist/>.

723

724 Yonghyeon Lee, Sangwoong Yoon, MinJun Son, and Frank C. Park. Regularized autoencoders for
 725 isometric representation learning. In *International Conference on Learning Representations*, 2022.
 726 URL <https://openreview.net/forum?id=mQxt817JL04>.

727

728 Alexander Lin and Alex Lu. Incorporating knowledge of plates in batch normalization improves
 729 generalization of deep learning for microscopy images. In David A Knowles, Sara Mostafavi, and
 730 Su-In Lee (eds.), *Proceedings of the 17th Machine Learning in Computational Biology meeting*,
 731 volume 200 of *Proceedings of Machine Learning Research*, pp. 74–93. PMLR, 21–22 Nov 2022.
 732 URL <https://proceedings.mlr.press/v200/lin22a.html>.

733

734 Yuhang Liu, Dong Gong, Yichao Cai, Erdun Gao, Zhen Zhang, Biwei Huang, Mingming Gong,
 735 Anton van den Hengel, and Javen Qinfeng Shi. I predict therefore i am: Is next token prediction
 736 enough to learn human-interpretable concepts from data?, 2025. URL <https://arxiv.org/abs/2503.08980>.

737

738 Francesco Locatello, Stefan Bauer, Mario Lucic, Gunnar Raetsch, Sylvain Gelly, Bernhard
 739 Schölkopf, and Olivier Bachem. Challenging common assumptions in the unsupervised learn-
 740 ing of disentangled representations. In Kamalika Chaudhuri and Ruslan Salakhutdinov (eds.),
 741 *Proceedings of the 36th International Conference on Machine Learning*, volume 97 of *Pro-
 742 ceedings of Machine Learning Research*, pp. 4114–4124. PMLR, 09–15 Jun 2019. URL
 743 <https://proceedings.mlr.press/v97/locatello19a.html>.

744

745 Francesco Locatello, Michael Tschannen, Stefan Bauer, Gunnar Rätsch, Bernhard Schölkopf, and
 746 Olivier Bachem. Disentangling factors of variations using few labels. In *International Conference*
 747 *on Learning Representations*, 2020.

748

749 Valentino Maiorca, Luca Moschella, Antonio Norelli, Marco Fumero, Francesco Locatello, and
 750 Emanuele Rodolà. Latent space translation via semantic alignment. In A. Oh, T. Nau-
 751 mann, A. Globerson, K. Saenko, M. Hardt, and S. Levine (eds.), *Advances in Neural*
 752 *Information Processing Systems*, volume 36, pp. 55394–55414. Curran Associates, Inc.,
 753 2023. URL https://proceedings.neurips.cc/paper_files/paper/2023/file/ad5fa03c906ca15905144ca3fbf2a768-Paper-Conference.pdf.

754

755 Emanuele Marconato, Sébastien Lachapelle, Sebastian Weichwald, and Luigi Gresele. All or
 756 none: Identifiable linear properties of next-token predictors in language modeling, 2025. URL
 757 <https://arxiv.org/abs/2410.23501>.

756 Loic Matthey, Irina Higgins, Demis Hassabis, and Alexander Lerchner. dsprites: Disentanglement
 757 testing sprites dataset. <https://github.com/deepmind/dsprites-dataset/>, 2017.
 758

759 Takeru Miyato, Toshiki Kataoka, Masanori Koyama, and Yuichi Yoshida. Spectral normalization for
 760 generative adversarial networks, 2018. URL <https://arxiv.org/abs/1802.05957>.
 761

762 Weili Nie, Tero Karras, Animesh Garg, Shoubhik Debnath, Anjul Patney, Ankit Patel, and Animashree
 763 Anandkumar. Semi-supervised StyleGAN for disentanglement learning. In Hal Daumé III and
 764 Aarti Singh (eds.), *Proceedings of the 37th International Conference on Machine Learning*, volume
 765 119 of *Proceedings of Machine Learning Research*, pp. 7360–7369. PMLR, 13–18 Jul 2020. URL
 766 <https://proceedings.mlr.press/v119/nie20a.html>.
 767

768 Beatrix M. G. Nielsen, Emanuele Marconato, Andrea Dittadi, and Luigi Gresele. When does
 769 closeness in distribution imply representational similarity? an identifiability perspective, 2025.
 770 URL <https://arxiv.org/abs/2506.03784>.
 771

772 Judea Pearl. Causal diagrams for empirical research. *Biometrika*, 82(4):669–688, 1995. ISSN
 773 00063444, 14643510. URL <http://www.jstor.org/stable/2337329>.
 774

775 F. Pedregosa, G. Varoquaux, A. Gramfort, V. Michel, B. Thirion, O. Grisel, M. Blondel, P. Pretten-
 776 hofer, R. Weiss, V. Dubourg, J. Vanderplas, A. Passos, D. Cournapeau, M. Brucher, M. Perrot, and
 777 E. Duchesnay. Scikit-learn: Machine learning in Python. *Journal of Machine Learning Research*,
 778 12:2825–2830, 2011.
 779

779 Patrik Reizinger, Szilvia Ujváry, Anna Mészáros, Anna Kerekes, Wieland Brendel, and Ferenc
 780 Huszár. Position: Understanding LLMs requires more than statistical generalization. In Ruslan
 781 Salakhutdinov, Zico Kolter, Katherine Heller, Adrian Weller, Nuria Oliver, Jonathan Scarlett, and
 782 Felix Berkenkamp (eds.), *Proceedings of the 41st International Conference on Machine Learning*,
 783 volume 235 of *Proceedings of Machine Learning Research*, pp. 42365–42390. PMLR, 21–27 Jul
 784 2024. URL <https://proceedings.mlr.press/v235/reizinger24a.html>.
 785

785 Patrik Reizinger, Randall Balestrieri, David Klindt, and Wieland Brendel. Position: An empirically
 786 grounded identifiability theory will accelerate self-supervised learning research, 2025a. URL
 787 <https://arxiv.org/abs/2504.13101>.
 788

788 Patrik Reizinger, Alice Bizeul, Attila Juhos, Julia E Vogt, Randall Balestrieri, Wieland Brendel,
 789 and David Klindt. Cross-entropy is all you need to invert the data generating process. In
 790 *The Thirteenth International Conference on Learning Representations*, 2025b. URL <https://openreview.net/forum?id=hrqNOxpItr>.
 791

791 Geoffrey Roeder, Luke Metz, and Durk Kingma. On linear identifiability of learned representations. In
 792 Marina Meila and Tong Zhang (eds.), *Proceedings of the 38th International Conference on Machine
 793 Learning*, volume 139 of *Proceedings of Machine Learning Research*, pp. 9030–9039. PMLR,
 794 18–24 Jul 2021. URL <https://proceedings.mlr.press/v139/roeder21a.html>.
 795

795 Bernard Russo. Maps which preserve equality of distance. must they be linear? Lecture notes, Full-
 796 ton College Colloquium, November 2017. URL <https://www.math.uci.edu/~brusso/slides111617full.pdf>.
 797

797 Maciej Sypetkowski, Morteza Rezanejad, Saber Saberian, Oren Kraus, John Urbanik, James Taylor,
 798 Ben Mabey, Mason Victors, Jason Yosinski, Alborz Rezazadeh Sereshkeh, Imran Haque, and
 800 Berton Earnshaw. Rxrx1: A dataset for evaluating experimental batch correction methods. In
 801 *Proceedings of the IEEE/CVF Conference on Computer Vision and Pattern Recognition (CVPR)
 802 Workshops*, pp. 4285–4294, June 2023.
 803

803 Joshua B. Tenenbaum, Vin de Silva, and John C. Langford. A global geometric framework for non-
 804 linear dimensionality reduction. *Science*, 290(5500):2319–2323, 2000. doi: 10.1126/science.290.
 805 5500.2319. URL <https://www.science.org/doi/abs/10.1126/science.290.5500.2319>.
 806

806 Jussi Vaisala. A survey of nearisometries, 2002. URL <https://arxiv.org/abs/math/0201098>.
 807

810 Julius Von Kügelgen, Yash Sharma, Luigi Gresele, Wieland Brendel, Bernhard Schölkopf, Michel
 811 Besserve, and Francesco Locatello. Self-supervised learning with data augmentations provably
 812 isolates content from style. *Advances in neural information processing systems*, 34:16451–16467,
 813 2021.

814
 815 Martin J. Wainwright and Michael I. Jordan. Graphical models, exponential families, and variational
 816 inference. *Foundations and Trends® in Machine Learning*, 1(1–2):1–305, 2008. ISSN 1935-8237.
 817 doi: 10.1561/2200000001. URL <http://dx.doi.org/10.1561/2200000001>.

818
 819 James C. R. Whittington, Will Dorrell, Surya Ganguli, and Timothy Behrens. Disentanglement with
 820 biological constraints: A theory of functional cell types. In *The Eleventh International Conference*
 821 *on Learning Representations*, 2023. URL https://openreview.net/forum?id=9Z_GfhZnGH.

822
 823 Lechao Xiao, Yasaman Bahri, Jascha Sohl-Dickstein, Samuel S. Schoenholz, and Jeffrey Penning-
 824 ton. Dynamical isometry and a mean field theory of cnns: How to train 10,000-layer vanilla
 825 convolutional neural networks, 2018. URL <https://arxiv.org/abs/1806.05393>.

826
 827 Dingling Yao, Dario Rancati, Riccardo Cadei, Marco Fumero, and Francesco Locatello. Unifying
 828 causal representation learning with the invariance principle, 2025. URL <https://arxiv.org/abs/2409.02772>.

829
 830 Guodong Zhang, Chaoqi Wang, Bowen Xu, and Roger Grosse. Three mechanisms of weight
 831 decay regularization. In *International Conference on Learning Representations*, 2019. URL
 832 <https://openreview.net/forum?id=B11z-3Rct7>.

833
 834 Roland S. Zimmermann, Yash Sharma, Steffen Schneider, Matthias Bethge, and Wieland Brendel.
 835 Contrastive learning inverts the data generating process. In Marina Meila and Tong Zhang
 836 (eds.), *Proceedings of the 38th International Conference on Machine Learning*, volume 139 of
 837 *Proceedings of Machine Learning Research*, pp. 12979–12990. PMLR, 18–24 Jul 2021. URL
 838 <https://proceedings.mlr.press/v139/zimmermann21a.html>.

839 840 A APPENDIX

841 A.1 A HISTORY OF THE TERM “IDENTIFIABILITY”

842
 843 **Statistical identifiability** Identifiability has a long history in statistics. For example, consider the
 844 following definition from Casella & Berger (2001) [p. 548], a canonical textbook in mathematical
 845 statistics:

846
 847 **Definition.** A parameter θ for a family of distributions $\{f(x | \theta) : \theta \in \Theta\}$ is
 848 identifiable if distinct values of θ correspond to distinct pdfs or pmfs. That is, if
 849 $\theta \neq \theta'$, then $f(x | \theta)$ is not the same function as $f(x | \theta')$.

850
 851 Our Definition 1 in the main text makes a straightforward generalization from likelihoods f to losses
 852 \mathcal{L} . Further, because of the dominance of empirical risk minimization and the fact that, unlike most
 853 likelihoods in statistical inference, losses are non-convex, we define identifiability at the minimizers
 854 of the expected loss. In other words, our definition of identifiability agrees with the statistical one,
 855 modulo some small changes to make it useful for talking about non-convex optimization, specifically
 856 the empirical minimization of non-convex risk functions. Indeed, this means that not only does
 857 Definition 1 agree with the statistical definition, but also other recent attempts at defining and proving
 858 representation identifiability results for practical machine learning models (Roeder et al., 2021;
 859 Reizinger et al., 2024).

860
 861 **Structural identifiability** On the other hand, there is a similarly long history of “structural identifi-
 862 ability” from econometrics. For example, consider Koopmans & Reiersøl (1950), which partly led to
 863 the Nobel prize:

864
 865 **Identifiability of structural characteristics by a model.** It is therefore a question
 866 of great practical importance whether a statement converse to the one just made is
 867 valid: can the distribution H of apparent variables, generated by a given structure
 868 S contained in a model \mathcal{S} , be generated by only one structure in that model?

869 Clearly, this is a different definition. Indeed, Koopmans & Reiersøl acknowledge that it is different
 870 from the statistical definition above. It implicitly assumes the existence of a “true model” S living
 871 within the estimable model class \mathcal{S} (and that this model generated the data), which flies in the face of
 872 mathematical statistics’ common quip “all models are wrong.”

873 Pearl (1995) inherits this definition, perhaps contributing to its later infusion into the ICA literature:
 874

875 **DEFINITION 4 (Identifiability).** The causal effect of X on Y is said to be
 876 identifiable if the quantity $P(Y|X)$ can be computed uniquely from any positive
 877 distribution of the observed variables that is compatible with a graph G .

879 Put simply, both these definitions of structural identifiability assume that the true data-generating
 880 process matches the model, and under this assumption, consider whether some structural parameter of
 881 interest can be identified. As a consequence, we refer to our Definition 2 as “structural identifiability”.
 882 The only generalization we make is that we do not specifically enumerate \mathcal{S} , or indeed require the
 883 true structure $S \in \mathcal{S}$. We do not enumerate \mathcal{S} because instead we enumerate Θ , the space of possible
 884 parameters of the neural network model, and specify the mapping F which generates the learned
 885 structure from a setting of the parameters $F : \theta \mapsto f_\theta$. We refer to the “true structure” as u . The
 886 relaxation of the requirement that the model class contains the “true structure” allows for other
 887 interesting cases, as illustrated in Example 2 below.

888 **Identifiability in linear ICA** Occasionally, these definitions of identifiability are used somewhat
 889 interchangeably. This is particular true in the case of recent developments in independent components
 890 analysis, such as extensions to the nonlinear mixing regime. Interestingly, the main result of the
 891 original seminal linear ICA paper (Comon, 1994) is a statistical identifiability result, not structural
 892 (we edit the quoted Corollary slightly so that it is self-contained):

894 **Corollary 13.** Let no noise be present in the linear ICA model with observations
 895 y , and define $y = Mx$ and $y = Fz$ for a random variable x with independent
 896 components such that at most one is Gaussian. Then if Ψ (a contrast function taking
 897 densities as inputs) is discriminant, $\Psi(p_x) = \Psi(p_z)$ if and only if $F = M\Lambda P$
 898 where Λ is an invertible diagonal matrix and P a permutation.

899 Of note, linear ICA is a case where most existing identifiability results depend on well-specification of
 900 the model. In particular, if the data is not generated by linear mixing from independent components,
 901 there is no guarantee that a linear decomposition into independent components exists (Castella
 902 et al., 2013) and therefore the statistical identifiability claim above is vacuous. In other words,
 903 there are few or no results available for statistical identifiability of linear ICA that don’t also imply
 904 structural identifiability. This perhaps helps explain why the two concepts have been used somewhat
 905 interchangeably in this area of the literature. However, as we will see in the examples below, this is
 906 not necessarily the case for all models of interest.

907 Notably, LiNGAM, a classical approach which extends linear ICA to causal discovery ?, provides
 908 an early example of this distinction between statistical and structural identifiability extending to
 909 graphical structures. In particular, they show that the independent components estimate can uniquely
 910 recover a causal graph under the assumption of linear functional relationships and additive noise
 911 (statistical identifiability). Structural identifiability follows under the assumption that a LiNGAM
 912 generated the data.

913
 914 **Identifiability in non-linear ICA** Noting that in general, non-linear extensions of ICA are impossi-
 915 ble (Locatello et al., 2019), recent works have attempted to find sets of assumptions that render the
 916 task tractable. One line of work utilizes side information, showing that independence conditional on
 917 this side information leads to identifiability (Khemakhem et al., 2020a). Notably, Khemakhem et al.
 918 (2020a) explicitly define their identifiability as statistical identifiability (up to an equivalence class),

918 but point out that if the true data-generating process takes the same form, structural identifiability of
 919 the true latents is achieved.
 920

921 Below, we show how two other examples fit into these definitions.
 922

923 **Example 1: mis-specified linear regression** The first example comes from traditional statistics.
 924 Consider the identifiability of the usual linear model $y = x^\top \beta + \eta'$ when the model is mis-specified
 925 in the sense that the true data-generating process is $y = f(x) + \eta'$ for some non-linear f . If f meets
 926 certain conditions, the following facts are true:
 927

- 928 1. β is statistically identifiable under the usual OLS assumptions (i.e. identifiable according to
 929 our Definition 1),
 930 2. f is not structurally identifiable (i.e., ϵ -nearly structurally identifiable with $\epsilon = 0$) according
 931 to Definition 2,
 932 3. the model is not absolutely identifiable according to Reizinger et al. (2025a), because the
 933 data-generating process does not match the model,
 934 4. a function h is structurally identifiable (i.e., ϵ -nearly with $\epsilon = 0$) according to our Definition
 935 2, where h is in some sense the “nearest” linear function to f .
 936

937 We emphasize that in this first example, we do not exploit the ϵ -nearness relaxation in our definitions,
 938 only the distinction between statistical and structural identifiability.
 939

940 **Example 2: masked autoencoders under imperfect reconstruction** Now, consider observations
 941 generated by some arbitrary non-linear mixing of latent factors $X = g(Z)$. For a masked autoencoder,
 942 the following facts *could* be true all at once, such as in the case of imperfect reconstruction:
 943

- 944 1. the internal representations given by the encoder f are statistically identifiable according to
 945 our Definition 1,
 946 2. the true data-generating process g is not structurally identifiable according to Definition 2
 947 because of imperfect reconstruction, but
 948 3. some approximation to the data-generating process h is structurally identifiable, but $h \neq g$
 949 because masked training prevents perfect reconstruction, so
 950 4. the model is not necessarily absolutely identifiable according to Reizinger et al. (2025a),
 951 depending on the assumptions on h and g (i.e. they might not reside in the same set of
 952 possible models).
 953

954 In this case, we might not have the simple analytical form for h that we do in Example 1, but it’s clear
 955 that *something* about the data-generating process is structurally identifiable. We emphasize that our
 956 theory does not cover this case, because it requires a notion of “closeness” between h and g which is
 957 not necessarily obvious (nor is it necessarily covered by our conception of ϵ -nearness, because the
 958 similarity is in observation space, not representation space).
 959

960 In particular, Theorem 1 does not require perfect reconstruction to yield statistical identifiability
 961 (and there perhaps is structural identifiability of some process h which is the nearest near-isometric
 962 approximation to the manifold of masked inputs, although we don’t make this argument explicit),
 963 but Theorem 3 does require perfect reconstruction to yield structural identifiability of g . A similar
 964 observation can be made about statistical versus structural identifiability in exponential family models
 965 like GPTs, as discussed in Appendix A.3.1.
 966

967 A.2 THEORY ROADMAP

968 We provide a brief table of contents to this set of appendices, which cover our theoretical contributions.
 969

- 970 • In Appendix A.3.1, we show the utility of our Definition 1 by showing that the statistical identifiability
 971 result from Roeder et al. (2021) meets our definition of statistical identifiability for the
 972 penultimate layer of exponential family models such as GPTs.
 973 • In Appendix A.3.2, we prove Theorem 1, our key statistical near-identifiability result up to $\mathcal{H}_{\text{rigid}}$
 974 for the internal representations of general self-supervised models.
 975

- In Appendices A.3.3 and A.3.4 we provide model-specific treatments for masked autoencoders and GPTs, showing that Theorem 1 holds for these models.
- In Appendix A.3.5, we prove Theorem 2, showing that linear ICA can resolve the rigid indeterminacy left by Theorem 1 (or indeed any other linear identifiability result), yielding statistical near-identifiability up to \mathcal{H}_σ (the space of signed permutations).
- In Appendix A.3.6, we prove Theorem 3, showing that for bi-Lipschitz data-generating processes, statistical near-identifiability extends to structural near-identifiability.
- In Appendix A.4, we show that the dynamical isometry condition used for characterizing practical neural network training regimes implies the bi-Lipschitz assumption necessary for Theorem 1.
- In Appendix A.5, we prove that structural identifiability (Definition 2) is strictly stronger than statistical identifiability (Definition 1), including in the ϵ -near case provided the transformation class \mathcal{H} is bounded.

A.3 PROOFS

A.3.1 STATISTICAL NEAR-IDENTIFIABILITY OF EXPONENTIAL FAMILY MODELS

The goal of this section is to contextualize two important statistical identifiability results (Roeder et al., 2021) which apply to the penultimate layer of exponential family models, discussed in Section 3.1 (“Connection with prior results”). Specifically, we show that the result of Roeder et al. (2021) meets the requirements of our Definition 1, and explain how the result of Nielsen et al. (2025) relates to our definitions. In particular, we are interested in models which have losses taking the form in Equation 1 from Section 3.1:

$$\mathcal{L}_\theta(x, y) = -\eta_\theta(x)^\top \mathbf{t}_\theta(y) + A_\theta(x) = -\log q_\theta(y \mid x)$$

where θ are the parameters of the model and η_θ give the representations of interest. The key result of Roeder et al. (2021) hinges on the assumption of sufficient diversity, which in the case of next-token predictors is the condition that the final linear classification head is in some sense “full rank”.

First, we prove a simple lemma showing that sufficient diversity can be recast as a mild property of the data distribution, combined with an assumption on the model.

Definition A.3. *The mapping $\mathbf{t} : \mathcal{Y} \rightarrow \mathbb{R}^D$ satisfies sufficient diversity with respect to $\mathbf{P}(x, y)$ if repeated sampling from the marginal distribution $y_d \sim \mathbf{P}(y)$ yields D linearly independent vectors $\{\mathbf{t}(y_d) - \mathbf{t}(y_0)\}_{d=1}^D$ for some $y_0 \in \mathcal{Y}$.*

Lemma A.1. *$\mathbf{t} : \mathcal{Y} \rightarrow \mathbb{R}^D$ satisfies the sufficient diversity assumption with respect to $\mathbf{P}(y)$ if and only if $\text{Cov}[\mathbf{t}(y)] \succeq \eta$ for some $\eta > 0$.*

Proof. Assume \mathbf{t} satisfies the sufficient diversity assumption. Let $v \in \mathbb{R}^D$ be any nonzero vector. By linear independence, we have $v^\top (\mathbf{t}(y_d) - \mathbf{t}(y_0)) \neq 0$ almost surely for any fixed y_0 , and therefore $v^\top \mathbf{t}(y) \neq c$ almost surely for any constant $c \in \mathbb{R}$. Thus, $v^\top \text{Cov}[\mathbf{t}(y)]v = \text{Var}[v^\top \mathbf{t}(y)] > 0$ as required.

To see the other direction, note that any D draws from the distribution $\mathbf{P}(\mathbf{t}(y))$ are linearly independent almost surely by the positive definiteness of the covariance matrix. \square

To see why this condition on the data distribution is extremely mild, note that even if $\mathbf{P}(y)$ is a finite categorical distribution over labels, so long as there are at least D of them, it is possible that \mathbf{t} satisfies sufficient diversity. Therefore, it is best regarded as a condition on the model. Now, we can state the key result of Roeder et al. (2021) as a lemma.

Lemma A.2. *(Theorem 1 of Roeder et al. (2021)) Let $\mathbf{P}(x, y)$ be a data distribution, and let $\mathcal{M} = \{\mathcal{L}_\theta(x, y) = -\eta_\theta(x)^\top \mathbf{t}_\theta(y) + A(x) : \theta \in \Theta\}$ be a model with an exponential family loss. Then, if $\mathcal{L}_\theta = \mathcal{L}_{\theta'}$ almost everywhere with respect to \mathbf{P} , we have that $\eta_\theta(x) = L\eta_{\theta'}(x)$ almost everywhere with respect to \mathbf{P} for some $L \in \mathcal{H}_{\text{linear}}$ whenever \mathbf{t}_θ and $\mathbf{t}_{\theta'}$ satisfy Definition A.3.*

The only additional requirement to meet our definition of ϵ -near-identifiability (Definition 1) is that Θ is sufficiently rich to approximate a unique minimum of the loss. We make this concrete in the

1026 following definition. Importantly, this assumption is *not* equivalent to requiring that the true data
 1027 distribution is in the model. Instead, it amounts to an assumption that the pointwise projection of
 1028 the true conditional $\mathbf{P}(y | x)$ onto the space of exponential family distributions is unique and in the
 1029 model. It turns out that this projection exists and is unique under the sufficient diversity assumption,
 1030 together with very mild assumptions on the data distribution. Therefore, this parallels the situation of
 1031 statistical identifiability of masked autoencoders (see Appendix A.3.3 and Appendix A.1, Example
 1032 2), where perfect reconstruction is not required for statistical identifiability (but might be required for
 1033 a notion of structural identifiability).

1034 **Definition A.4.** *For an exponential family loss $\mathcal{L}_\theta(x, y) = -\eta_\theta(x)^\top \mathbf{t}_\theta(y) + A_\theta(x)$, a data distribu-
 1035 tion $\mathbf{P}(x, y)$, and a sufficient statistics function \mathbf{t} satisfying sufficient diversity, consider the following
 1036 minimization problems:*

$$1037 \kappa^*(x) = \arg \min_{\kappa \in \mathcal{K}} KL(\mathbf{P}(y | x) || \mathbf{Q}_\kappa)$$

1038 where $\mathbf{Q}_\kappa(y) = \kappa^\top \mathbf{t}(y) + A(\kappa)$ is the approximating distribution. Then, a parameter space Θ of an
 1039 exponential family model of the form in Equation 1 is sufficiently rich to exactly model the minimizer
 1040 if this minimizer exists for every x , is unique for almost every x with respect to $\mathbf{P}(x)$, and there exists
 1041 $\theta \in \Theta$ such that $\eta_\theta(x) = \kappa^*(x)$.
 1042

1043 **Remark.** For categorical likelihoods, the only requirement on the true data distribution $\mathbf{P}(y | x)$ is
 1044 that all categories must have positive probability for the above to hold (for almost every x). This
 1045 means that the assumption is trivially satisfied for e.g. GPT-class models assuming that any token
 1046 might be next for any given state. This condition is called minimality (Wainwright & Jordan, 2008).

1047 Now we give the full statement of the proposition showing that the Lemma A.2 combines with the
 1048 above assumption to yield ϵ -near-identifiability in expectation according to our definition (with $\epsilon = 0$).
 1049

1050 **Proposition A.1.** *Let $\mathbf{P}(x, y)$ be a data distribution, and let $\mathcal{M} = \{\mathcal{L}_\theta(x, y) = -\eta_\theta(x)^\top \mathbf{t}_\theta(y) +$
 1051 $A_\theta(x) : \theta \in \Theta\}$ be a model with an exponential family loss. Then, for $F : \theta \mapsto \eta_\theta$, $(\mathbf{P}, \mathcal{M}, F)$ is
 1052 identifiable in expectation up to $\mathcal{H}_{\text{linear}}$ when the label distribution $\mathbf{P}(y)$ is sufficiently diverse and
 1053 the approximating class Θ is sufficiently rich according to Definition A.4.*
 1054

1055 *Proof.* Minimizing the expected loss of the model via empirical risk minimization is equivalent to
 1056 minimizing the following cross-entropy:
 1057

$$1058 \begin{aligned} 1059 \arg \min_{\theta \in \Theta} \mathbb{E}_{x, y \sim \mathbf{P}} [\mathcal{L}_\theta(x, y)] &= \arg \min_{\theta \in \Theta} \mathbb{E}_{x, y \sim \mathbf{P}} [-\log q_\theta(y | x)] \\ 1060 &= \arg \min_{\theta \in \Theta} \mathbb{E}_{x \sim \mathbf{P}} [\text{CE}(q_\theta(y | x) || \mathbf{P}(y | x))] \end{aligned}$$

1062 where $-\log q_\theta(y | x) \propto -\eta_\theta(x)^\top \mathbf{t}_\theta(y) + A_\theta(x)$ parameterizes an exponential family approximating
 1063 class. By sufficient richness, call q_{θ^*} the unique distribution induced by any minimizer θ^* . So, for
 1064 any two minimizers θ, θ' we have $\mathcal{L}_\theta = \mathcal{L}_{\theta'}$ almost everywhere and Lemma A.2 yields identifiability
 1065 in expectation (Definition 1, see Remark) as required. \square
 1066

1067 Nielsen et al. (2025) extends this result to the case where it is not guaranteed that $q_\theta = q_{\theta'}$ for any
 1068 two optimizers θ, θ' . For example, this might arise due to the sufficient richness condition not being
 1069 met, or due to imperfect optimization. Instead, a closeness condition can be placed on q_θ and $q_{\theta'}$,
 1070 yielding a notion that is similar to our notion of statistical ϵ -near-identifiability. However, we note
 1071 that Nielsen et al. (2025) does not aim to characterize the optima of a particular loss, instead relaxing
 1072 this requirement to cover any procedure yielding likelihoods. This makes it an interesting extension
 1073 of Roeder et al. (2021) in a different direction than ours.
 1074

1075 A.3.2 RIGID NEAR-IDENTIFIABILITY OF MODELS WITH BI-LIPSCHITZ MAPPINGS

1076 We begin by briefly outlining the approach for proving Theorem 1. The key idea is to leverage modern
 1077 results in isometric approximation (Vaisala, 2002; Alestalo et al., 2001). In particular, consider the
 1078 latent spaces of two models which produce the same outputs. Call the mappings from latents to
 1079 outputs in these two models g and g' . If the mapping from latent to output is invertible, we can “stitch

1080 together” the latent spaces of the two models by a single function $g^{-1} \circ g'$. So, $g^{-1} \circ g'$ **maps the**
 1081 **representations of an input under one model to its representations in the other model.**

1082
 1083 We assume that both g and g' are locally bi-Lipschitz, meaning that distances between nearby
 1084 points are not too badly deformed, and that g and g' are smooth C^1 diffeomorphisms. When this
 1085 is the case, $g^{-1} \circ g'$ is also locally bi-Lipschitz and smooth, and therefore nearly an isometry, with
 1086 “nearly” determined by the bi-Lipschitz constants. The convexity of the latent spaces yields global
 1087 bi-Lipschitzness with the same bounds.

1088 The isometric approximation theory outlined in (Vaisala, 2002; Alestalo et al., 2001) then tells us how
 1089 far $g' \circ g^{-1}$ is from an actual isometry, and allows us to construct bounds accordingly. Isometries on
 1090 \mathbb{R}^D are rigid transformations, and together, these facts yield near-identifiability up to $\mathcal{H}_{\text{rigid}}$.

1091 We rely on the following definition of locally bi-Lipschitz, which allows us to treat latent-to-observable
 1092 mappings which might induce manifold structure in the ambient space, allowing the taking of a
 1093 tighter constant L . In what follows, $\|\cdot\|$ denotes the usual ℓ_2 norm unless otherwise stated.

1094 **Definition A.5.** *A function $f : \mathcal{Z} \rightarrow \mathbb{R}^N$ is locally $(1 + L)$ -bi-Lipschitz if for every $\mathbf{z} \in \mathcal{Z} \subset \mathbb{R}^D$,
 1095 there exists an open neighbourhood $U_{\mathbf{z}} \ni \mathbf{z}$ such that for all $\mathbf{z}' \in U_{\mathbf{z}}$, we have*

$$1097 \quad \frac{1}{1 + L} \|\mathbf{z} - \mathbf{z}'\| \leq \|f(\mathbf{z}) - f(\mathbf{z}')\| \leq (1 + L) \|\mathbf{z} - \mathbf{z}'\|$$

1100 When $L = 0$, distances are preserved exactly, a notion referred to as *isometry*. When the bi-Lipschitz
 1101 constraint is global (i.e., holds for any $U \subset \mathcal{Z}$) and \mathcal{Z} is bounded, there is a nice relationship between
 1102 the bi-Lipschitz property and the notion of a *near-isometry*, which allows for additive distortion of
 1103 distances.

1104 **Definition A.6.** *A function $f : \mathcal{Z} \rightarrow \mathbb{R}^N$ for $\mathcal{Z} \subset \mathbb{R}^D$ is an ε -near-isometry if for every $\mathbf{z}, \mathbf{z}' \in \mathcal{Z}$
 1105 we have $\|\mathbf{z} - \mathbf{z}'\| - \varepsilon \leq \|f(\mathbf{z}) - f(\mathbf{z}')\| \leq \|\mathbf{z} - \mathbf{z}'\| + \varepsilon$.*

1106 In particular, if f is globally $(1 + L)$ -bi-Lipschitz, we have that f is also an ε -near-isometry where
 1107 $\varepsilon = \Delta L$ where $\Delta = \sup_{\mathbf{z}, \mathbf{z}' \in \mathcal{Z}} \|\mathbf{z} - \mathbf{z}'\|$ is the diameter of \mathcal{Z} .

1108 We require two lemmas to prove our main statistical identifiability result Theorem 1. The first is a
 1109 fundamental result which shows that distance-preserving transformations on e.g. Euclidean spaces
 1110 (or convex subsets thereof) are always rigid motions.

1111 **Lemma A.3.** *(Mazur-Ulam Theorem, Russo (2017)) Let \mathcal{Z} and \mathcal{Z}' be closed, convex subsets of \mathbb{R}^D
 1112 with non-empty interior. Then, if $f : \mathcal{Z} \rightarrow \mathcal{Z}'$ is a bijective isometry, then f is affine.*

1113 We also leverage the following more recent result (see Vaisala (2002) for a history of isometric
 1114 approximation) which shows that near-isometric mappings (such as $(1 + L)$ -bi-Lipschitz functions
 1115 on bounded domains) have bounded deviation from a truly isometric mapping.

1116 **Lemma A.4.** *(Near-Isometries are Near Isometries, Theorem 2.2 of Alestalo et al. (2001)) Suppose
 1117 $\mathcal{Z}, \mathcal{Z}' \subset \mathbb{R}^D$ with \mathcal{Z} compact and $f : \mathcal{Z} \rightarrow \mathcal{Z}'$ is a ΔL -near-isometry, where $\Delta = \sup_{\mathbf{z}, \mathbf{z}' \in \mathcal{Z}} \|\mathbf{z} - \mathbf{z}'\|$.
 1118 Then, there exists an isometry $U : \mathbb{R}^D \rightarrow \mathbb{R}^D$ such that $\sup_{\mathbf{z} \in \mathcal{Z}} \|U(\mathbf{z}) - f(\mathbf{z})\| \leq c_D \sqrt{L} \Delta$.*

1119 With these two tools in hand, we can provide an intuitive overview of the assumptions required and a
 1120 concrete statement of Theorem 1, proving statistical near-identifiability of the representations.

1121 **Assumption Summary.** We assume that the representations have convex support (i.e., the pushfor-
 1122 ward of $\mathbf{P}(x)$ by any encoder f_{θ} has convex support). We assume that any “decoder” g_{θ} is injective,
 1123 smooth (in particular, at least C^1), and is locally bi-Lipschitz with constant $1 + L$. Note that injectivity,
 1124 smoothness, and local bi-Lipschitzness of g_{θ} (with any constant) implies that g_{θ} is diffeomorphic
 1125 onto its image.

1126 **Theorem.** *Let $\mathbf{P}(x)$ be a data distribution, and let \mathcal{M} be a model with a parameter space Θ . Let
 1127 $F : \theta \mapsto f_{\theta}$, $G : \theta \mapsto g_{\theta}$ and $H : \theta \mapsto g_{\theta} \circ f_{\theta}$, where g_{θ} is a smooth diffeomorphism and the
 1128 pushforward of \mathbf{P} through f_{θ} has convex support. Then, if $(\mathbf{P}, \mathcal{M}, H)$ is statistically identifiable
 1129 in expectation, then $(\mathbf{P}, \mathcal{M}, F)$ is statistically ϵ -near identifiable in expectation up to $\mathcal{H}_{\text{rigid}}$ for
 1130 $\epsilon = c_D \sqrt{2L + L^2} \Delta$ where $1 + L$ is a local bi-Lipschitz constant bound for g_{θ} , and c_D and Δ are
 1131 constants independent of the model (and L).*

1134 *Proof.* Let θ and θ' be optima of the infinite-data limit of the empirical risk minimization problem
 1135 for \mathcal{M} with respect to \mathbf{P} .

1136 Without loss of generality, assume that $f_\theta(\mathbf{x}) = 0 = f_{\theta'}(\mathbf{x})$ for some $\mathbf{x} \in \text{supp } \mathbf{P}$, noting that
 1137 translating the latent spaces of both models do not alter any of our hypotheses. Then, by the
 1138 identifiability of $(\mathbf{P}, \mathcal{M}, H)$, we have that $T = g_{\theta'}^{-1} \circ g_\theta$ satisfies $T(0) = 0$, is clearly smooth and
 1139 diffeomorphic onto its image, and is therefore globally $(1 + L)^2$ -bi-Lipschitz by the convexity and
 1140 compactness of the latent spaces and is a $\Delta(L^2 + 2L)$ -near-isometry where $\Delta = \sup_{\mathbf{x}, \mathbf{x}' \in \mathcal{X}} \|f_\theta(\mathbf{x}) -$
 1141 $f_\theta(\mathbf{x}')\|$ is the diameter of the latent manifold. Furthermore, we have that $T \circ f_\theta = f_{\theta'}$. By the above
 1142 fact about bi-Lipschitz functions and Lemma A.4, we have that there exists an isometry U such that
 1143

1144

$$\begin{aligned} 1145 \text{ess sup}_{p(x)} \|f_{\theta'}(\mathbf{x}) - U(f_\theta(\mathbf{x}))\|_2 &= \text{ess sup}_{p(x)} \|T(f_\theta(\mathbf{x})) - U(f_\theta(\mathbf{x}))\|_2 \\ 1146 &\leq c_D \sqrt{2L + L^2} \Delta \end{aligned}$$

1147

1148 where c_D is a constant depending on D . By convexity of the latent spaces and the Mazur-Ulam
 1149 theorem for convex bodies (Lemma A.3), $U \in \mathcal{H}_{\text{rigid}}$ as required. \square
 1150

1151 **Remark.** The constant c_D depends only on the latent dimension D and can be computed by the
 1152 following recursive formulae given in Alestalo et al. (2001):
 1153

1154

1155

$$\begin{aligned} 1156 \varrho_1 &= 3.3 \\ 1157 \tau_1 &= 6.2 \end{aligned}$$

1158

$$\begin{aligned} 1159 \gamma_1(t)^2 &= 0.1 + (t + \sqrt{t^2 + 6.2})^2 \\ 1160 \varrho_{n+1}(\lambda) &= 3.02 + \tau_n(\lambda) \sqrt{1 + \tau_n(\lambda)/\lambda^2} + \sum_{k=1}^n \varrho_k(\lambda) (2 + \varrho_k(\lambda)/\lambda^2) \\ 1161 \tau_{n+1}(\lambda) &= \tau_n(\lambda) + \varrho_{n+1}(\lambda) (2 + \varrho_{n+1}(\lambda)/\lambda^2) \\ 1162 \gamma_{n+1}(t) &= \min\{\max\{\gamma_n(\lambda), \beta_{n+1}(\lambda, t)\} : \lambda > 0\} \\ 1163 \beta_{n+1}(\lambda, t)^2 &= 0.1 + (t + \sqrt{t^2 + \tau_{n+1}(\lambda)})^2 + \lambda^{-2} \sum_{k=2}^{n+1} \varrho_k(\lambda)^2 \end{aligned}$$

1164

1165

1166

1167

1168

1169

1170

1171

1172

1173

with $c_D = \gamma_D(0)$ for any D . As an example, $c_3 \approx 18.8$.

A.3.3 MODEL-SPECIFIC RESULTS: MASKED AUTOENCODERS

The following assumptions are sufficient for a masked autoencoder to meet the criteria of Theorem 1.

1174

1175

1176

1177

1178

1179

1180

1181

1182

1183

1184

Model. A **masked autoencoder** consists of a distribution $\mathbf{P}(m)$ defined over a space of masking
 functions $\mathcal{N} = \{m : \mathcal{X} \rightarrow \tilde{\mathcal{X}}\}$, an encoder $f_\theta : \mathcal{X} \cup \tilde{\mathcal{X}} \rightarrow \mathbb{R}^D$, and a decoder $g_\theta : \mathbb{R}^D \rightarrow \mathbb{R}^N$,
 where we assume $\mathcal{X} \subset \mathbb{R}^N$ is compact. For convenience, we write $h = g_\theta \circ f_\theta$. The loss function
 with respect to a data point x and mask m is $\mathcal{L}_{\text{MAE}}(h; m, x) = \|h(m(x)) - x\|^2$. We assume that
 $\tilde{\mathcal{X}}$ is sequentially dense in $\mathcal{X} \cup \tilde{\mathcal{X}}$, and that marginalizing the joint distribution over the masks and
 data $\mathbf{P}(m, x, m(x))$ yields a distribution $\mathbf{P}(m(x))$ with full support on $\tilde{\mathcal{X}}$. Further, we assume that
 at the optimum, g_θ is diffeomorphic and locally $(1 + L)$ -bi-Lipschitz for some constant $L \geq 0$.
 Finally, we assume that the image of \mathcal{X} pushed forward through the encoder is convex, and that the
 parameterization of h is continuous on $\mathcal{X} \cup \tilde{\mathcal{X}}$ and \mathcal{M} is sufficiently rich to contain the function
 which attains the optimal value of the loss, as derived below.

1185

1186

1187

1188

1189

1190

1191

1192

1193

1194

1195

1196

1197

1198

1199

1200

1201

1202

1203

1204

1205

1206

1207

1208

1209

1210

1211

1212

1213

1214

1215

1216

1217

1218

1219

1220

1221

1222

1223

1224

1225

1226

1227

1228

1229

1230

1231

1232

1233

1234

1235

1236

1237

1238

1239

1240

1241

1242

1243

1244

1245

1246

1247

1248

1249

1250

1251

1252

1253

1254

1255

1256

1257

1258

1259

1260

1261

1262

1263

1264

1265

1266

1267

1268

1269

1270

1271

1272

1273

1274

1275

1276

1277

1278

1279

1280

1281

1282

1283

1284

1285

1286

1287

1288

1289

1290

1291

1292

1293

1294

1295

1296

1297

1298

1299

1300

1301

1302

1303

1304

1305

1306

1307

1308

1309

1310

1311

1312

1313

1314

1315

1316

1317

1318

1319

1320

1321

1322

1323

1324

1325

1326

1327

1328

1329

1330

1331

1332

1333

1334

1335

1336

1337

1338

1339

1340

1341

1342

1343

1344

1345

1346

1347

1348

1349

1350

1351

1352

1353

1354

1355

1356

1357

1358

1359

1360

1361

1362

1363

1364

1365

1366

1367

1368

1369

1370

1371

1372

1373

1374

1375

1376

1377

1378

1379

1380

1381

1382

1383

1384

1385

1386

1387

1388

1389

1390

1391

1392

1393

1394

1395

1396

1397

1398

1399

1400

1401

1402

1403

1404

1405

1406

1407

1408

1409

1410

1411

1412

1413

1414

1415

1416

1417

1418

1419

1420

1421

1422

1423

1424

1

conditional expectation exists and is unique almost everywhere in $\tilde{\mathcal{X}}$. In particular, we have the following expression:

$$\mathbb{E}[x \mid \tilde{x}] = \frac{\int_{\mathcal{X}} x \mathbf{P}(x) \mathbf{P}[m(x) = \tilde{x}] dx}{\int_{\mathcal{X}} \mathbf{P}(x) \mathbf{P}[m(x) = \tilde{x}] dx} \quad (2)$$

Then under the masked autoencoding model, $\hat{f}(\tilde{x}) = \mathbb{E}[x \mid \tilde{x}]$ is the unique minimizer of \mathcal{L}_{MAE} by the standard fact that the conditional mean estimate minimizes the mean squared error loss. By the continuity of \hat{f} on $X \cup \tilde{X}$ and sequential density of $\tilde{\mathcal{X}}$ in $\mathcal{X} \cup \tilde{\mathcal{X}}$, consider an arbitrary sequence in $\tilde{\mathcal{X}}$, $\tilde{x}_n \rightarrow x \in \mathcal{X}$, noting that $\hat{f}(x) = \lim_{\tilde{x}_n \rightarrow x} \hat{f}(\tilde{x}_n)$ is well-defined, unique, and agrees regardless of the choice of sequence. Note that this continuity is by hypothesis. We remark that it would be of interest to study properties of $\mathbf{P}(m)$ which lead to conditional expectation operators with certain properties including continuity. \square

Remark. *We emphasize that any such minimizer is also a minimizer when an arbitrary subsetting operation applied to both the prediction and the target, such as the usual subsetting to masked tokens in the loss for computational efficiency.*

A.3.4 MODEL-SPECIFIC RESULTS: GPTs & SUPERVISED LEARNERS

The results for earlier-layer representations of GPTs and supervised learners take advantage of the penultimate-layer identifiability result in Proposition A.1. We formalize this with the assumptions below.

Model. Let \mathbf{P} and \mathcal{M} be a model satisfying Proposition A.1, with $F : \theta \mapsto f_\theta$ yielding the representation function of interest, $G : \theta \mapsto g_\theta$ yielding the map between the outputs of f_θ and the penultimate layer. Let $1 + L$ be a bound on the bi-Lipschitz constant of the smooth diffeomorphism g_θ , and suppose the pushforward of \mathbf{P} through f_θ has convex support.

Proof. By Proposition A.1, we have statistical identifiability in expectation up to $\mathcal{H}_{\text{linear}}$ of (\mathbf{P}, M, H) for $H : \theta \mapsto g_\theta \circ f_\theta$. Thus, Theorem 1 applies. \square

A.3.5 INDEPENDENT COMPONENTS ANALYSIS IN LATENT SPACE

We consider the class of independent components analysis algorithms which optimize a contrast function, such as fastICA (Hyvärinen & Oja, 2000). In general, fastICA enjoys good convergence properties despite a lack of guarantees, and even in the face of mis-specification (Castella et al., 2013). Of particular concern in our setting is mis-specification of the kind such that there exists no orthogonal transformation in which the components are truly independent. This assumption is non-trivial to assess, and furthermore sufficient but not necessary for convergence (Castella et al., 2013), so we opt for something more relaxed, aimed at practical optimization. Specifically, we show that near-isometries are simple enough functions that they do not substantially alter the recovered components when ICA converges well, in the sense that they preserve well-differentiated optima.

Model. For an encoder f with whitened outputs $\hat{f}(x)$, independent components analysis consists of maximizing the contrast $\mathcal{J} = \sum_{d=1}^D J(\mathbf{q}_d^T \hat{f}(x))$ where J is a contrast function, over $(\mathbf{q}_1, \dots, \mathbf{q}_D)^T = Q \in \mathbb{SO}(D)$, the space of special orthogonal matrices. As a technical condition, we require $\sup_f \|\text{Cov}[f(x)]\| \geq \lambda$ for some $\lambda > 0$, where the supremum is over any possible encoder (latents must have bounded correlation). The contrast function J must be C^2 with $|J'(y)| \leq L_1$ and $|J''(y)| \leq L_2$ for rigid transformations of elements of a convex body $y = Uf(x)$. The optima of the ICA objective \mathcal{J} must also be locally convex for $f(x)$, in the sense that for sufficiently large samples the Riemannian Hessian $\text{Hess}_Q \mathcal{J} \succcurlyeq \mu$ for some $\mu > 0$ at the optimum, under any perturbation of the data not larger than ε . Finally, the only indeterminacy to the optima of an individual ICA problem must be the usual invariances: signed permutations in \mathcal{H}_σ .

Under these conditions, we can show that ε -nearness does not introduce any further complications to the identifiability of the ICA model. We begin with a brief lemma about the stability of the whitening operation which typically precedes contrast-based ICA.

1242 **Lemma A.5.** *Let X and X' be zero-mean random vectors in \mathbb{R}^D such that $\|X - X'\| \leq \varepsilon$ almost
 1243 surely and $\|X\|, \|X'\| \leq a$ almost surely. Furthermore, suppose the smallest eigenvalues of the
 1244 covariance of X and X' are bounded below by $\lambda > 0$. Let $W = \Sigma^{-1/2}$ and $W' = \Sigma'^{-1/2}$ be the
 1245 usual whitening matrices for X and X' respectively. Then $\|W'X' - WX\| \leq C\varepsilon$ almost surely
 1246 where $C = \lambda^{-1/2}(1 + \lambda^{-1}a^2)$.*

1247
 1248 *Proof.* First, note that we have the following bound almost surely:
 1249

$$\begin{aligned} \|XX^T - X'X'^T\| &\leq \|X(X - X')^T + (X - X')X'^T\| \\ &\leq \|X\|\varepsilon + \|X'\|\varepsilon \leq 2a\varepsilon \end{aligned}$$

1250
 1251
 1252 Taking expectations yields $\|\Sigma - \Sigma'\| \leq 2a\varepsilon$. Now, using the resolvent equation $B^{-1} - A^{-1} = B^{-1}(B - A)A^{-1}$, we have the following bound on the difference in operator norms of W and W' :
 1253
 1254

$$\begin{aligned} \|W' - W\| &= \|\Sigma^{-1/2} - \Sigma'^{-1/2}\| \\ &\leq \|W'\|\|\Sigma^{1/2} - \Sigma'^{1/2}\|\|W\| \\ &\leq \frac{\|\Sigma' - \Sigma\|}{2\lambda^{3/2}} \\ &\leq \frac{a\varepsilon}{\lambda^{3/2}} \end{aligned}$$

1255
 1256 where the second-to-last inequality follows from the fact that the matrix square root is $(1/(2\sqrt{\lambda}))$ -
 1257 Lipschitz when $\lambda > 0$. Operating on the desired norm directly:
 1258
 1259

$$\begin{aligned} \|W'X' - WX\| &\leq \|W'X' - W'X + W'X - WX\| \\ &\leq \|W'(X' - X)\| + \|(W' - W)X\| \\ &\leq \frac{\varepsilon}{\sqrt{\lambda}} + \frac{a^2\varepsilon}{\lambda^{3/2}} \end{aligned}$$

1260 almost surely so the proposition holds. □
 1261
 1262

1263 The next lemma simplifies the exposition of our main theorem. We show that PCA resolves the
 1264 first-order dependence structure (i.e. the non-rigid component of linear transformations), leaving only
 1265 a rigid transformation to be resolved by ICA.
 1266

1267 **Lemma A.6.** *Suppose there exists functions $f, f' : \mathcal{X} \rightarrow \mathcal{Z}$ such that for $p(x)$ supported on \mathcal{X} , we
 1268 have $\mathbb{E}_{\mathbf{P}(x)}[f(x)] = \mathbb{E}_{\mathbf{P}(x)}[f'(x)] = 0$, full-rank covariance of $f(x)$ and $f'(x)$, and furthermore
 1269 $\sup_{x \in \mathcal{X}}\|f(x) - Af'(x)\| \leq \varepsilon$ for some invertible matrix A with positive determinant and $\varepsilon \geq 0$.
 1270 Then, there exists $U \in \mathcal{H}_{\text{rigid}}$ such that $\sup_{x \in \mathcal{X}}\|\hat{f}(x) - U\hat{f}'(x)\| \leq C\varepsilon$ where \hat{f}, \hat{f}' are the whitened
 1271 outputs of f and f' respectively, $U \in \mathcal{H}_{\text{rigid}}$, and $C = \lambda_A^{-1/2}\lambda^{-1/2}\left(1 + \frac{\Lambda_A^2}{\lambda_A\lambda}a^2\right)$ where Λ_A and λ_A
 1272 are the largest and smallest singular values of A respectively, λ is a lower bound on the smallest
 1273 eigenvalues of the covariance of $f(x)$ and $f'(x)$, and $\|f(x)\|, \|f'(x)\| \leq a$ almost surely with respect
 1274 to $\mathbf{P}(x)$.*

1275
 1276 *Proof.* Denote and $W = \Sigma^{-1/2}$ and $W' = \Sigma'^{-1/2}$ the usual whitening matrices for f and f'
 1277 respectively. Let W_A be any whitening matrix for Af' . Let $U = W_AAW'^{-1}$. Then U is orthogonal
 1278 (and can be made to have determinant 1 with a sign flip by the freedom to choose W_A) because
 1279 $UU^T = W_AAW'^{-1}W'^{-T}A^TW_A = W_A\Sigma'_AW_A^T = I$, and we have:
 1280

1296

1297

$$\begin{aligned}
\|\hat{f}(x) - U\hat{f}'(x)\| &= \|Wf(x) - W_A AW'^{-1}\hat{f}'(x)\| \\
&= \|Wf(x) - W_A Af'(x)\| \\
&\leq \lambda_A^{-1/2} \lambda^{-1/2} \left(1 + \frac{\Lambda_A^2}{\lambda_A \lambda} a^2\right) \varepsilon
\end{aligned}$$

1303

1304

1305

1306

1307

almost surely with respect to $\mathbf{P}(x)$ where the final line follows by application of the previous lemma to the usual whitening matrices. The determinant of U is positive by the fact that the usual whitening matrices can be made unique by selecting their positive definite forms and A has positive determinant, so $U \in \mathcal{H}_{\text{rigid}}$. \square

1308

1309

1310

1311

Lemma A.7. (Implicit Function Theorem, de Oliveira (2014) Theorem 2) Let $F \in C^1(\Omega; \mathbb{R}^m)$ where $\Omega \subset \mathbb{R}^N \times \mathbb{R}^m$ is open. Suppose there exists a point $(a, b) \in \Omega$ such that $F(a, b) = 0$ and $\frac{\partial F}{\partial y}(a, b)$ is invertible, where y represents the part of the argument f in \mathbb{R}^m . Then, there exists an open set $X \subset \mathbb{R}^n$ such that $a \in X$ and an open set $Y \subset \mathbb{R}^m$ such that $b \in Y$ and:

1312

- For each $x \in X$, there is a unique $y = f(x) \in Y$ such that $F(x, f(x)) = 0$

1313

- $f(a) = b$ and f is C^1 with $Df(x) = -\left(\frac{\partial F}{\partial y}(x, f(x))\right)^{-1} \left(\frac{\partial F}{\partial x}(x, f(x))\right)$ for all $x \in X$

1314

1315

1316

Finally, this lemma shows the crux of our argument: if ICA converges well in any pair of latent spaces, the solutions can't differ too much.

1317

1318

1319

1320

1321

1322

Lemma A.8. (Finite-Sample ICA Under Perturbations) Consider whitened observations $\{\mathbf{x}_n\}_{n=1}^N$ and corruptions $\{\varepsilon_n\}_{n=1}^N$ (such that the corrupted observations $\mathbf{y}_n = \mathbf{x}_n + \varepsilon_n$ are also whitened) both in \mathbb{R}^D such that $\|\mathbf{x}_n\| \leq a$ and $\|\varepsilon_n\| \leq b$ for all $n = 1, \dots, N$. Let Q_* denote a stationary point of the optimization problem

1323

1324

1325

$$\max_{Q \in \mathbb{SO}(D)} \frac{1}{N} \sum_{n=1}^N \sum_{d=1}^D J(\mathbf{q}_d^T \mathbf{x}_n)$$

1326

Then, there exists a stationary point $Q_*(\varepsilon_1, \dots, \varepsilon_N)$ of the perturbed optimization problem

1327

1328

1329

1330

1331

1332

$$\max_{Q \in \mathbb{SO}(D)} \frac{1}{N} \sum_{n=1}^N \sum_{d=1}^D J(\mathbf{q}_d^T (\mathbf{x}_n + \varepsilon_n))$$

1333

1334

1335

1336

such that $\|Q_* \mathbf{x}_n - Q_*(\varepsilon_1, \dots, \varepsilon_N)(\mathbf{x}_n + \varepsilon_n)\| \leq C + b$ for all N where $C = \frac{L_2(a+b) + \sqrt{D}L_1}{\mu} ab$. Furthermore, $PQ_*(\varepsilon_1, \dots, \varepsilon_N)$ is a stationary point of the perturbed optimization problem attaining the same value for any signed permutation matrix $P \in \mathcal{H}_\sigma$ such that $\det P = 1$.

1337

1338

1339

1340

Proof. We treat $\mathbb{SO}(D)$ as a Riemannian manifold and consider the properties of the perturbed optimization problem. For notational convenience, write $\varepsilon = (\varepsilon_1, \dots, \varepsilon_N)^T$ noting that then $\|\varepsilon\| \leq \sqrt{N}b$.

1341

1342

1343

We consider first the Euclidean gradient with respect to Q , where we write the perturbed sample as $\mathbf{y}_n = \mathbf{x}_n + \varepsilon_n$. Denote $\mathbf{g}_n(Q) = (J'(\mathbf{q}_1^T \mathbf{y}_n), \dots, J'(\mathbf{q}_D^T \mathbf{y}_n))^T$ for any n . Then:

1344

1345

1346

1347

$$\nabla_Q \mathcal{J}(Q, \varepsilon) = \frac{1}{N} \sum_{n=1}^N \mathbf{g}_n(Q) \mathbf{y}_n^T$$

1348

1349

The tangent space at a point $Q \in \mathbb{SO}(D)$ can be parameterized by the vector space of skew-symmetric matrices. Denoting $\text{skew}(A) = \frac{1}{2}(A - A^T)$, the Riemannian gradient is given by the projection of $\nabla_Q \mathcal{J}$ onto the tangent space:

1350

1351
$$\text{grad}_Q \mathcal{J}(Q, \varepsilon) = Q \text{skew}(Q^T \nabla_Q \mathcal{J}(Q, \varepsilon))$$
 1352

1353 With this machinery, we can apply the Euclidean implicit function theorem (IFT). Let $Q_* \in \mathbb{SO}(D)$
1354 be an unperturbed optimum. Adopt the matrix exponential parameterization in a neighbourhood
1355 about Q_* , i.e., let $\gamma : N \rightarrow \mathbb{SO}(D)$ be given by $\gamma(\Omega) = Q_* \exp(\Omega)$ for some sufficiently small
1356 $N \subset \mathbb{R}^{D(D-1)/2}$ for the map to be injective. Let
1357

1358
$$F(\varepsilon, \Omega) = \text{grad}_Q \mathcal{J}(\gamma(\Omega), \varepsilon) = \gamma(\Omega) \text{skew}(\gamma(\Omega)^T \nabla_Q \mathcal{J}(\gamma(\Omega), \varepsilon))$$
 1359

1360 and apply the IFT to F , noting that the hypotheses hold at $\Omega = 0$ and $\varepsilon = 0$. We thus have some
1361 neighbourhoods $E \subset \mathbb{R}^{N \times D}$ and $O \subset \mathbb{R}^{D(D-1)/2}$ such that for any $\varepsilon \in E$ there exists $\Omega_*(\varepsilon) \in O$
1362 such that
1363

1364
1365
$$\|D_{\varepsilon_n} \Omega_*(\varepsilon_n)\|_F = \|\text{Hess}_Q^{-1} \mathcal{J}(\gamma(\Omega_*(\varepsilon)), \varepsilon)\| \left\| \frac{\partial F}{\partial \varepsilon}(\varepsilon, \Omega_*(\varepsilon)) \right\|$$

1366
1367
1368
1369
1370
1371
1372
1373
1374

$$\begin{aligned} &\leq \frac{1}{\mu} \left\| \text{skew} \left(\gamma(\Omega)^T \frac{\partial \nabla_Q \mathcal{J}}{\partial \varepsilon_n} \right) \right\| \\ &\leq \frac{1}{\mu} \left\| \frac{\partial \nabla_Q \mathcal{J}}{\partial \varepsilon_n} \right\| \\ &\leq \frac{L_2(a+b) + L_1\sqrt{D}}{\mu N} \end{aligned}$$

1375 Here, the bound on the Hessian comes by hypothesis, while the second term follows from the fact
1376 that the skew operator and multiplication by an orthogonal matrix is norm-preserving, combined with
1377 the following expression for the Euclidean directional cross-derivative:
1378

1379
$$\partial_{\varepsilon_n} \nabla_Q \mathcal{J}[\mathbf{h}] = \frac{1}{N} ((R_n(Q)Q\mathbf{h})\mathbf{y}_n^T + \mathbf{g}_n(Q)\mathbf{h}^T)$$
 1380
1381

1382 where $R_m(Q) = \text{diag}\{J''(\mathbf{q}_1^T \mathbf{y}_m), \dots, J''(\mathbf{q}_D^T \mathbf{y}_m)\}$ and we have $\|\partial_{\varepsilon_n} \nabla_Q \mathcal{J}[\mathbf{h}]\| \leq$
1383 $\frac{L_2(a+b) + \sqrt{D}L_1}{N}$ as required. Aggregating across all n , we have $\|D_{\varepsilon} \Omega_*(\varepsilon)\|_F \leq \frac{L_2(a+b) + L_1\sqrt{D}}{\mu\sqrt{N}}$.
1384 By hypothesis, the additive symmetry between \mathbf{x}_n and ε_n is sufficient for this bound to hold for any
1385 sufficiently small perturbation.
13861387 As a result, we have
1388

1389
1390
$$\begin{aligned} \|Q_*(\varepsilon)(\mathbf{x}_n + \varepsilon_n) - Q_*(0)\mathbf{x}_n\| &\leq \|Q_*(\varepsilon) - Q_*(0)\| \|\mathbf{x}_n\| + \|Q_*(\varepsilon)\varepsilon_n\| \\ &\leq \|\Omega_*(\varepsilon) - \Omega_*(0)\| \|\mathbf{x}_n\| + b \\ &\leq \frac{(L_2(a+b) + L_1\sqrt{D})ab}{\mu} + b \end{aligned}$$
 1391
1392
1393
1394

1395 as required. □
13961397 Below, we provide a complete overview of the assumptions we make for Theorem 2.
13981399 **Assumption Summary.** We assume that the representation distribution (i.e. the pushforward of $\mathbf{P}(x)$
1400 by any encoder f_θ) has full-rank covariance, and that the support of the distribution has diameter
1401 bounded by Δ . The eigenvalues of the covariance matrices are assumed to be bounded below by
1402 λ . Furthermore, we assume that the identifiability up to $\mathcal{H}_{\text{linear}}$ of $(\mathbf{P}, \mathcal{M}, F)$ (where $F : \theta \mapsto f_\theta$)
1403 is satisfied for linear maps with singular values bounded between λ_A and Λ_A . Finally, we assume
1404 that the contrast function used for ICA is Lipschitz (with constant L_1) and has Lipschitz derivative

(with constant L_2), and that ICA converges such that the Riemannian Hessian at the optimum has eigenvalues bounded below by $\mu > 0$.

With these lemmata, Theorem 2 in the main text follows easily.

Theorem. Suppose $(\mathbf{P}, \mathcal{M}, F)$ is ϵ -nearly identifiable up to $\mathcal{H}_{\text{linear}}$ for $F : \theta \mapsto f_\theta$. Then, a new model \mathcal{M}' which applies whitening and contrast function-based independent components analysis to the latent representations given by f_θ is ϵ' -near-identifiable up to \mathcal{H}_σ for $\epsilon' = K\epsilon + K'\epsilon^2$, where K and K' are constants free of ϵ that depends on the maximum diameter of the latent space Δ , the spectra of the covariance matrix of the representations, and the properties of the ICA contrast function.

Proof. Let f_θ and $f_{\theta'}$ be two optimal encoders. By ϵ -near identifiability up to $\mathcal{H}_{\text{linear}}$, there exists A such that $\text{ess sup}_{\mathbf{P}(x)} \|f_\theta(x) - Af_{\theta'}(x)\| \leq \epsilon$. If A has positive determinant, Lemma A.6 with the usual whitening applied to both encoders yields $C\epsilon$ -near-identifiability up to $\mathcal{H}_{\text{rigid}}$ for $C = \lambda_A^{-1/2} \lambda^{-1/2} \left(1 + \frac{\Lambda_A^2}{\lambda_A \lambda} a^2\right)$. If not, the sign of a single latent can be flipped, which flips the sign of a single column of A , allowing the application of Lemma A.6. Denote the whitened encoders by $\widehat{f}_\theta(x)$ and $\widehat{f}_{\theta'}(x)$. Lemma A.8 then applies with $a = \Delta$ and $b = C\epsilon$, where Δ is the maximum diameter of any latent space, yielding a bound $C' = \frac{L_2(\Delta+C\epsilon)+\sqrt{D}L_1}{\mu} \Delta C\epsilon$. Taking the limit as $N \rightarrow \infty$ and denoting $\widehat{f}_\theta^{\text{ICA}}(x)$ and $\widehat{f}_{\theta'}^{\text{ICA}}(x)$ the outputs of the encoders with whitening and ICA applied, we have $\text{ess sup}_{\mathbf{P}(x)} \|\widehat{f}_\theta^{\text{ICA}}(x) - P\widehat{f}_{\theta'}^{\text{ICA}}(x)\| \leq K\epsilon + K'\epsilon^2$ for $K = \frac{L_2\Delta^2 C + \sqrt{D}L_1\Delta C}{\mu}$ and $K' = \frac{L_2 C^2 \Delta}{\mu}$, and the indeterminacy $P \in \mathcal{H}_\sigma$ arises by the fact that any signed permutation of the latents is a maximum of the ICA objective, as required. \square

A.3.6 STRUCTURAL NEAR-IDENTIFIABILITY VIA ICA

Here, we are able to give a short proof of Theorem 3 by leveraging identical arguments to the proof of Theorem 2.

Assumption Summary. We assume that the representation distribution (i.e. the pushforward of $\mathbf{P}(x)$ by any encoder f_θ) has full-rank covariance, and that the support of the distribution has diameter bounded by Δ . The eigenvalues of the covariance matrices are assumed to be bounded below by λ . Furthermore, we assume that the identifiability up to $\mathcal{H}_{\text{linear}}$ of $(\mathbf{P}, \mathcal{M}, F)$ (where $F : \theta \mapsto f_\theta$) is satisfied for linear maps with singular values bounded between λ_A and Λ_A . Finally, we assume that the contrast function used for ICA is C^2 with Lipschitz first (with constant L_1) and second (with constant L_2) derivatives, and that ICA converges such that the Riemannian Hessian at the optimum has eigenvalues bounded below by $\mu > 0$. Finally, the end-to-end model $g_\theta \circ f_\theta$ must reconstruct its inputs perfectly at the optimum and the true data-generating process g must be $(1 + \delta)$ -bi-Lipschitz, smooth, and injective (and therefore diffeomorphic onto its image), with the data-generating factors being white (i.e. zero mean, unit variance), being non-Gaussian and having independent components. Finally, we assume that Θ is sufficiently rich so that $u \in \mathcal{M}$, i.e., the model can approximate the ground-truth data-generating structure.

Theorem. Let $\mathbf{P}(u)$ be some multivariate distribution with independent non-Gaussian components with zero mean and unit **variance**, and consider data $\mathbf{P}(x)$ generated by pushforward through a smooth diffeomorphism g such that g is $(1 + \delta)$ -bi-Lipschitz. Let \mathcal{M} be a model with a sufficiently rich parameter space Θ . Let $F : \theta \mapsto f_\theta$, $G : \theta \mapsto g_\theta$ and $H : \theta \mapsto g_\theta \circ f_\theta$. Then, if $(\mathbf{P}, \mathcal{M}, H)$ structurally identifies the identity function in expectation (i.e. attains perfect reconstruction), we have that $(\mathbf{P}, \mathcal{M}, F)$ ϵ -nearly identifies the structure g^{-1} up to $\mathcal{H}_{\text{rigid}}$, and furthermore that a new model \mathcal{M}' which applies whitening and independent components analysis to the latent representations given by f_θ ϵ' -nearly identifies the structure g^{-1} up to \mathcal{H}_σ where ϵ and ϵ' depend on δ and Lipschitz bounds on g_θ , and ϵ' depends additionally on the spectrum of the covariance matrix of the representations and the properties of the ICA contrast function employed.

Proof. Take $\delta = \max\{\delta, L\}$ as the maximum of the two bi-Lipschitz constants of the data-generating process and the bound on the bi-Lipschitz constant of the decoders in the model class. Theorem 1 yields δ' -near-identifiability in expectation up to $\mathcal{H}_{\text{rigid}}$ for $\delta' = c_D \sqrt{2\delta + \delta^2} \Delta$. With the inverse of the true data-generating map taking the place of one of the encoders, the same argument from the

1458 proof of Theorem 1 yields the first claim, namely δ' -near structural identifiability of g^{-1} up to $\mathcal{H}_{\text{rigid}}$.
 1459

1460 The rest of the proof follows similarly to the proof of Theorem 2 in Appendix A.3.5, with the inverse
 1461 of the true data-generating map taking the place of one of the encoders. In particular, let θ be an
 1462 optimum and consider f_θ and g_θ . Without loss of generality, assume that $f_\theta(\mathbf{x}) = 0 = g^{-1}(\mathbf{x})$,
 1463 noting that the encoder f_θ and decoder g_θ can be translated arbitrarily without altering any of our
 1464 hypotheses. The same argument then applies, yielding the result. The precise constant is the same,
 1465 with $\epsilon = K\delta' + K'\delta'^2$ for K and K' as defined in the statement of Theorem 2. \square
 1466

1467 A.4 DYNAMICAL ISOMETRY AND BI-LIPSCHITZNESS

1469 **Proposition.** Suppose $f : \mathbb{R}^D \rightarrow \mathbb{R}^N$ is once differentiable and satisfies dynamical isometry, in the
 1470 sense that the singular values λ_i of the Jacobian J satisfy $|\lambda_i - 1| \leq \epsilon$ for $i = 1, \dots, \min\{D, N\}$
 1471 for some $1 > \epsilon \geq 0$. Then, f is locally L -bi-Lipschitz for $L = \frac{1+\epsilon}{1-\epsilon}$.
 1472

1473 *Proof.* Let $x, y \in \mathbb{R}^D$. Then the mean value theorem yields the bound $\|f(x) - f(y)\| \leq \|J_f\| \|x - y\| \leq (1 + \epsilon) \|x - y\|$. By the same argument, $(1 - \epsilon) \|x - y\| \leq \|f(x) - f(y)\|$, and taking $L = \frac{1+\epsilon}{1-\epsilon}$
 1474 (a bound on the condition number of J) yields a suitable bi-Lipschitz constant. \square
 1475

1476 **Remark.** Many popular regularization techniques spanning architectures and tasks optimize im-
 1477 plicitly or explicitly for dynamical isometry, with the level of evidence ranging from theoretical to
 1478 empirical. For example, weight decay has been shown theoretically and empirically to do so (Zhang
 1479 et al., 2019), normalization techniques in generative adversarial networks optimize for it directly
 1480 (Karras et al., 2020; Miyato et al., 2018), residual layers yield this property (Bachlechner et al.,
 1481 2020), and specialized techniques have been developed to yield it at initialization (Xiao et al., 2018).
 1482

1483 A.5 STRUCTURAL IDENTIFIABILITY IMPLIES STATISTICAL IDENTIFIABILITY

1485 Below, we prove that statistical (near)-identifiability is implied by structural (near)-identifiability.

1486 **Theorem.** Suppose $(\mathbf{P}, \mathcal{M}, F)$ δ -nearly identifies the structure u up to \mathcal{H} for $F : \theta \mapsto f_\theta$. Then,
 1487 $(\mathbf{P}, \mathcal{M}, F)$ is ϵ -nearly identifiable up to \mathcal{H} for some $\epsilon \in \mathbb{R}$ provided that \mathcal{H} is bounded by $C \in \mathbb{R}^+$
 1488 as in the sense of an operator norm.
 1489

1490 *Proof.* Let $\theta, \theta' \in \mathcal{S}$ be solutions to the minimization problem $\min_{\theta \in \Theta} \mathbb{E}[\mathcal{L}_\theta]$ where $\mathcal{M} = \{\mathcal{L}_\theta : \theta \in \Theta\}$. By structural identifiability, we have that there exist h and h' relating θ and θ' respectively
 1491 to u . More concretely, we have:
 1492

$$\begin{aligned} \|h \circ f_\theta - u\|_{L^p} &\leq \delta \\ \|h' \circ f_{\theta'} - u\|_{L^p} &\leq \delta \end{aligned}$$

1498 Take $h^* = h^{-1} \circ h'$, where the inverse and composition are well-defined because \mathcal{H} is a group of
 1499 functions mapping \mathbb{R}^D to itself. h^* can be understood as mapping $f_{\theta'}$ as close to f_θ as possible under
 1500 the available assumptions. Then, we have
 1501

$$\begin{aligned} \|f_\theta - h^* \circ f_{\theta'}\|_{L^p} &= \|h^{-1} \circ h \circ f_\theta - h^{-1} \circ h' \circ f_{\theta'}\|_{L^p} \\ &= \|h^{-1} \circ h \circ f_\theta - h^{-1} \circ u + h^{-1} \circ u - h^{-1} \circ h' \circ f_{\theta'}\|_{L^p} \\ &\leq \|h^{-1}\|_{\text{op}} (\|h \circ f_\theta - u\|_{L^p} + \|h' \circ f_{\theta'} - u\|_{L^p}) \\ &\leq 2C\delta \end{aligned}$$

1508 where the third line follows by the triangle inequality, and the final line by structural identifiability of
 1509 u and boundedness of \mathcal{H} , yielding the result.
 1510

1511 The constant C arises because solutions might exist on a different scale from the data-generating
 1512 process u (and therefore from each other). Partly as a result of this fact, this theorem likely is

1512 not useful for certain identifiability classes such as $\mathcal{H}_{\text{linear}}$, which even if bounded by assumption
 1513 can likely yield more fruitful identifiability results via a direct approach. On the other hand, for
 1514 identifiability classes like $\mathcal{H}_{\text{rigid}}$, the bound is in some sense tight.

1515 Finally, we emphasize that the result is largely agnostic to the choice of reasonable norms, although
 1516 we have in mind the usual operator norm and an L^p norm for $1 \leq p \leq \infty$, taken with respect to the
 1517 data distribution $\mathbf{P}(x)$. \square

1519 **Remark.** Taking $\delta = 0$ shows that structural identifiability implies statistical identifiability in
 1520 expectation.

1522 **A.6 CONFORMAL MAPS AS NEAR-ISOMETRIES**

1524 In this section we make rigorous the arguments outlined in Section 3.3.1. First, we outline the
 1525 mollification argument which allows us to take derivatives in L^2 without hassle.

1527 **Mollification** Let ϕ_{σ^2} be the isotropic zero-mean Gaussian density with variance σ^2 . For any
 1528 image represented by a function F , note that $F_\sigma = F * \phi_{\sigma^2}$ is a “smooth” version of that image
 1529 without hard edges. Accordingly, mollifying all images by the same Gaussian means that taking
 1530 the Gateaux derivative of image-valued functions becomes possible in L^2 , and only introduces a
 1531 multiplicative constant dependent on the variance σ^2 which we would like to ignore. To see that this
 1532 is possible, consider the data-generating process for a square articulating along the x -axis according
 1533 to a coordinate p outlined in Section 3.3.1:

$$1534 \\ 1535 f(p) = [(x, y) \mapsto \mathbf{1}_{|x-p| \leq r, |y| \leq r}] \in L^2([-1, 1]) \\ 1536$$

1537 Denote $f_\sigma(p) = f(p) * \phi_{\sigma^2}$. Then, convolving with the distributional derivative gives

$$1539 \\ 1540 f'_\sigma(p) = \mathbf{1}_{|y| \leq |r|} (\phi(x - p - r) - \phi(x - p + r)) \\ 1541 \\ 1542 \|f'_\sigma(p)\|_{L^2}^2 = \frac{2r}{\sqrt{\pi\sigma}} + \mathcal{O}(\exp(-\sigma^2)) \\ 1543$$

1544 Pick any two distinct latents p_0 and p_1 . For any smoothed manifold, we have that their geodesic
 1545 distance is given by $\left(\frac{2r}{\sqrt{\pi\sigma}} + \mathcal{O}(\exp(-\sigma^2))\right) |p_1 - p_0|$. The distance between any two points can
 1546 then be “renormalized” against this distance by dividing through it, ensuring that as $\sigma \rightarrow 0$ what is
 1547 left is a constant. This then implies that what we are actually computing in the subsequent sections is
 1548 not a metric inherited from the L^2 norm at all, but rather defines a whole new geodesic distance on
 1549 the limiting manifold of unsmoothed images. For notational clarity, we ignore mollification in the
 1550 rest of this section and return to a heuristic argument for the next sections. We direct the interested
 1551 reader to Grimes (2003), Section 2.6 for a fully rigorous treatment.

1553 **Two-dimensional manifold** Now, we fully characterize the 2-dimensional manifold described in
 1554 the main text. Let $\mathcal{Z} = \{(p, r) \mid a \leq p \leq b, R_0 \leq r \leq R\}$ denote the manifold of latent variables of
 1555 the position of the square and its half-side length. Each point $\mathbf{z} \in \mathcal{Z}$ can be identified with an image:

$$1557 \\ 1558 f(p, r) = [(x, y) \mapsto \mathbf{1}_{|x-p| \leq r, |y| \leq r}] \in L^2([-1, 1]) \\ 1559$$

1560 **Directional derivatives** The derivative with respect to p remains the same as in the main text, and
 1561 the derivative with respect to r follows similarly:

$$1562 \\ 1563 \\ 1564 \|\partial_p f(p, r)\|^2 = 2r \\ 1565 \|\partial_r f(p, r)\|^2 = 8r$$

1566 However, checking that f is a conformal map also demands that $\partial_p f$ and $\partial_r f$ are orthogonal in L^2 .
 1567 To see this, note that finite difference approximation to $\partial_p f$ are the (negative) left and (positive)
 1568 right edges of the square, while the finite difference approximation to $\partial_r f$ are all (positive) edges
 1569 of the square. Therefore, the top edges contribute nothing to the inner product $\langle \partial_p f, \partial_r f \rangle$ while the
 1570 contributions of the left and right edges cancel. Thus, the Riemannian metric can be written
 1571

$$1572 \quad G(p, r) = 2r \begin{pmatrix} 1 & 0 \\ 0 & 4 \end{pmatrix}$$

$$1573 \quad G(p', r') = r' I$$

1574 where the reparameterization $p' = p/4$ and $r' = 2r$ allows us to recover the isotropy.
 1575

1576 **Near-isometry** It remains to show how f can be viewed as locally bi-Lipschitz. To see this, note
 1577 that we have the following global bound on the differential:
 1578

$$1582 \quad 2R_0\|\mathbf{u}\| \leq \|Df(\mathbf{u})\| \leq 2R\|\mathbf{u}\|$$

1583 for \mathbf{u} in the tangent space at any point along \mathcal{Z} . Accordingly, we have the following bound on the
 1584 geodesic distance:
 1585

$$1587 \quad \sqrt{2R_0}\|\mathbf{z}_1 - \mathbf{z}_0\| \leq d_{\text{geo}}(f(\mathbf{z}_1), f(\mathbf{z}_0)) \leq \sqrt{2R}\|\mathbf{z}_1 - \mathbf{z}_0\|$$

1589 where d_{geo} is the geodesic distance along the image manifold. As a result (assuming w.l.o.g. that
 1590 $R_0 \leq 1$), f is locally $\sqrt{R/R_0}$ -bi-Lipschitz. Furthermore, for any f_*^{-1} from the image manifold to
 1591 a convex subset of \mathbb{R}^2 which is also $\sqrt{R/R_0}$ -bi-Lipschitz, $f \circ f_*^{-1}$ is globally R/R_0 -bi-Lipschitz
 1592 (with respect to the ℓ^2 norm on both spaces, where the constant follows by convexity) and is therefore
 1593 a near-isometry with constant $(R/R_0 - 1)\Delta$ where $\Delta = \sqrt{4(R - R_0)^2 + (a - b)^2}$ is simply the
 1594 diameter of \mathcal{Z} .
 1595

1596 A.7 EXPERIMENTAL DETAILS

1598 A.7.1 WARMUP EXPERIMENT: MNIST

1600 We conducted experiments on the MNIST dataset (LeCun & Cortes, 2010) to validate our theoretical
 1601 predictions regarding the identifiability of latent representations as a function of the bi-Lipschitz
 1602 constant of the decoder.
 1603

1604 **Training** We trained pairs of orthogonal LeakyReLU autoencoders with the following architecture:
 1605

- 1606 • **Encoder:** $\mathbb{R}^{784} \rightarrow \mathbb{R}^{784} \rightarrow \mathbb{R}^{784} \rightarrow \mathbb{R}^{784} \rightarrow \mathbb{R}^2$
- 1607 • **Decoder:** $\mathbb{R}^2 \rightarrow \mathbb{R}^{784} \rightarrow \mathbb{R}^{784} \rightarrow \mathbb{R}^{784} \rightarrow \mathbb{R}^{784}$

1608 All linear layers used orthogonal weight parametrization (no
 1609 bias terms). LeakyReLU activations with leak constant $\alpha \in$
 1610 $\{0.0, 0.25, 0.5, 0.75, 0.9, 1.0\}$ were applied at all intermediate
 1611 layers. The latent dimension was $D = 2$. All models were fit
 1612 using the Adam optimizer (Kingma & Ba, 2015) with learning
 1613 rate $\eta = 5 \times 10^{-4}$ for up to 2000 epochs, minimizing the mean
 1614 squared reconstruction error. Early stopping was applied with
 1615 patience of 50 epochs and minimum improvement threshold
 1616 of 10^{-6} . Gradients were clipped to unit norm for stability. We
 1617 repeated each configuration with 10 random seeds for robust-
 1618 ness, yielding $6 \times 10 = 60$ experimental runs. We filtered
 1619 experimental runs to exclude poorly converged autoencoders.
 Specifically, we removed runs where the reconstruction error

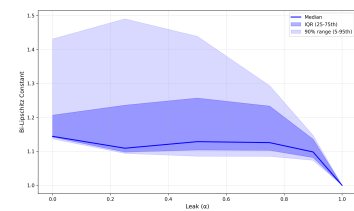


Figure A.3: The distribution of sample-level bi-Lipschitz constant estimates $B(z)$ tightens around 1 as $\alpha \rightarrow 0$.

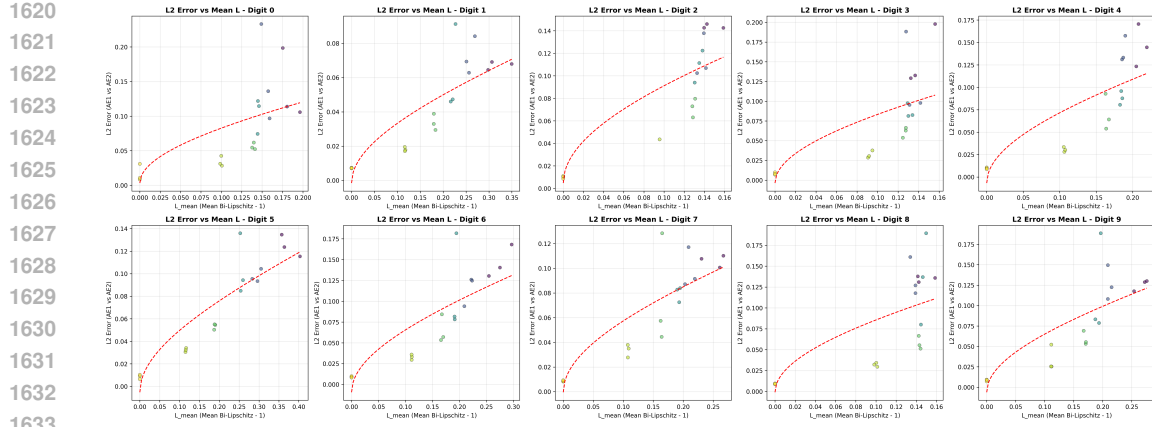


Figure A.6: In digit-specific models, controlling the bi-Lipschitz constant L leads to improved identifiability (reduced ℓ_2 error) with pattern similar to the full-dataset models.

of either autoencoder exceeded the 95th percentile observed at the reference leak value $\alpha = 0.9$. This removed 11/60 runs.

Results For a given autoencoder, we compute the representations z of a random subset of 1000 samples. For the decoder g , the bi-Lipschitz constant at a given latent point z is given as

$$B(z) = \max_v \{\|J_g(z)v\|_2, 1/\|J_g(z)\|_2\}$$

where the maximum is taken over 10 randomly sampled unit vectors. We plot the distribution of $B(z)$ as a function of the leak constant α in Figure A.3. As $\alpha \rightarrow 1$, the distribution is typically well-concentrated around a mean not much larger than one, with a relatively small number of outliers. Figure 2 (in the main text) plots the samplewise estimate of $L = \mathbb{E}_{P(z)}[B(z) - 1]$ versus identifiability. Although more robust to outliers, this is not a formal bound because Theorem 1 relies on a global L , i.e. $L = \max_{P(z)}[B(z) - 1]$. For completeness, we plot using the maximum in Figure A.4, with the maximum taken over all 1000 samples. Both plots include fitted curves of the form $\ell_2 \text{ error} = a\sqrt{L + L^2} + b$ to the identifiability measurements, consistent with the theorem.

As $\alpha \rightarrow 1$, the estimated bi-Lipschitz constants L do indeed shrink toward 1 as expected. This suggests validity of the experimental testbed, but not Theorem 1 itself. However, as $L \rightarrow 1$, we see that identifiability does indeed improve significantly (ℓ_2 error $\rightarrow 0$) as predicted by the Theorem. Notably, this is despite the fact that perfect reconstruction does not hold (Figure A.5).

We also completed the same experiment with a model per digit. This allows us to assess whether class-level indeterminacies play a role in identifiability in this problem setting like in (Nielsen et al., 2025). All hyperparameters and setup remains the same, except we fit three seeds per digit for a total of $10 \text{ digits} \times 6 \text{ leak values} \times 3 \text{ seeds} = 180$ runs. Filtering using the same rule for reconstruction removed 5/180 runs. Results are consistent for these per-digit autoencoders as well, suggesting that for this setting of hyperparameters, class-level indeterminacies do not play a substantial role in the level of empirical identifiability (Figure A.6).

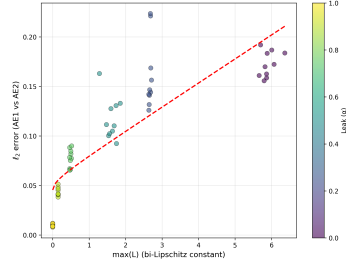


Figure A.4: Controlling the bi-Lipschitz constant L leads to improved identifiability (reduced ℓ_2 error). The proportionality does not appear to differ whether the max or mean bi-Lipschitz constant is estimated.

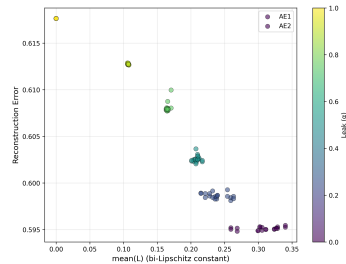


Figure A.5: Reconstruction error improves as the bi-Lipschitz constant grows (leak $\alpha \rightarrow 1$). Notably, poor reconstruction does not inhibit identifiability.

1674 A.7.2 MEASURING NEAR-IDENTIFIABILITY
16751676 We describe here the setup for the alignment experiments reported in Table 1. All reported statistics
1677 are *in-sample*, with representations taken from the same data on which the models were trained. For
1678 each model, we extract the following hidden states:1679

- 1680 • **GPT-class models (Pythia-160M):** penultimate-layer hidden states.
- 1681 • **MAE models:** latent representations obtained by averaging patch embeddings.
- 1682 • **Supervised models (ResNet-18):** penultimate-layer representations.

1683 We apply the following representation alignment techniques:
16841685

- 1686 • **Permutation:** representation dimensions were matched using the Hungarian algorithm to resolve
1687 signed permutation indeterminacies.
- 1688 • **Rigid:** estimated via the Procrustes algorithm with a global scaling constant (rigid similarity
1689 transform).
- 1690 • **Linear:** estimated via least-squares regression with no additional regularization or constraints.
- 1691 • **ICA:** estimated using FastICA (scikit-learn implementation), applied to the full representation
1692 dimension with all components retained. The Hungarian algorithm resolves the remaining signed
1693 permutation in latent space.

1694 Alignment quality is reported as the mean per-example ℓ_2 error, normalized by the *latent diameter*,
1695 defined as the maximum pairwise ℓ_2 distance among representations. For ICA, efficiency is reported
1696 as the proportion of error reduction relative to the supervised rigid transform:

1697
$$1698 \text{ICA efficiency} = \frac{\text{Permutation} - \text{ICA}}{\text{Permutation} - \text{Rigid}}.$$

1699

1700 A.7.3 DISENTANGLEMENT EXPERIMENTS
17011702 We reproduce only the autoencoder (AE) results, enough to validate that we obtain similar perfor-
1703 mance, and apply ICA to these models. Specifically, each hyperparameter setting is re-fit 3 times,
1704 and training step where the average performance is the best is selected (according to modularity, after
1705 filtering for reconstruction as in Hsu et al. (2023)).1706 As in the original experiments in Hsu et al. (2023), the latent spaces are overparameterized with the
1707 number of latents equal to twice the number of ground-truth sources $n_z = 2n_s$. As a result, the latent
1708 space is rank deficient. To avoid the introduction of additional hyperparameters for pruning inactive
1709 latents which could bias the performance of our approach (via e.g. whitening with dimensionality
1710 reduction), we fit the FastICA model without whitening. Inspection of the decoder Jacobian reveals
1711 that inactive latents are obvious (corresponding singular values are very near zero) and the remaining
1712 components of the Jacobian have similar scale (likely due to high weight decay), suggesting that
1713 full-rank whitening would have minimal impact here except to drive up the noise from inactive latents.
1714 As a result, we perform no whitening and preserve all latent dimensions.1715 Table 5 is an augmented version of Table 2, with standard errors computed across the 3 models with
1716 the best hyperparameter setting for each model. Results for all models other than AE (reproduction)
1717 and AE + ICA are quoted from Hsu et al. (2023), which averaged over 5 seeds instead of 3.1718 A.7.4 OPENPHENOM EXPERIMENTS
17191720 The whitening and FastICA Hyvärinen & Oja (2000) algorithms are from the `scikit-learn`
1721 package Pedregosa et al. (2011). These models are trained at the patch level on the patches from the
1722 first channel of images in Rxrx3-core Kraus et al. (2025), where patches are specifically subsampled
1723 from the top left-hand corner. To ensure computational feasibility, a single patch is sampled from
1724 each image, yielding approximately 222K patches. Both models use the default hyperparameters (all
1725 principal components are kept and the contrast function is $\log \cosh$).1726 Gradient boosting models are trained using LightGBM Ke et al. (2017) (hyperparameters in Table
1727 6). Models are trained to predict whether the image patch embedding is from an image which is
1728 perturbed or not. Models are evaluated using area under the receiver operator characteristic curve.

1728
 1729 A separate model is trained on each plate, which is then evaluated on all remaining plates. Below, we
 1730 report an augmented version of Table 3 with the standard error of the mean computed across folds.
 1731 When more than one independent experiment (corresponding to a guide) is available for a given gene,
 1732 the standard error is computed across all folds from all guides.

1733 Gene	1734 Mean AUROC \pm s.e. (\uparrow)				1735 Sparsity \pm s.e. (\uparrow more sparse)			
	1736 Base	1737 PCA	1738 PCA + ICA	1739 PCA + Rand	1740 Base	1741 PCA	1742 PCA + ICA	1743 PCA + Rand
CYP11B1 (1)	0.663 \pm 0.008	0.692 \pm 0.008	0.709 \pm 0.005	0.678 \pm 0.010	0.184 \pm 0.006	0.204 \pm 0.007	0.237 \pm 0.006	0.188 \pm 0.007
EIF3H (1)	0.682 \pm 0.008	0.724 \pm 0.004	0.749 \pm 0.007	0.725 \pm 0.003	0.192 \pm 0.004	0.224 \pm 0.010	0.268 \pm 0.008	0.214 \pm 0.006
HCK (1)	0.670 \pm 0.012	0.693 \pm 0.007	0.711 \pm 0.005	0.668 \pm 0.007	0.156 \pm 0.004	0.208 \pm 0.004	0.241 \pm 0.006	0.166 \pm 0.005
MTOR (6)	0.663 \pm 0.003	0.690 \pm 0.003	0.705 \pm 0.003	0.679 \pm 0.003	0.166 \pm 0.002	0.201 \pm 0.003	0.233 \pm 0.003	0.186 \pm 0.002
PLK1 (6)	0.803 \pm 0.002	0.811 \pm 0.002	0.815 \pm 0.002	0.792 \pm 0.002	0.251 \pm 0.003	0.307 \pm 0.004	0.305 \pm 0.003	0.262 \pm 0.003
SRC (1)	0.660 \pm 0.004	0.694 \pm 0.007	0.706 \pm 0.004	0.676 \pm 0.007	0.170 \pm 0.006	0.214 \pm 0.003	0.240 \pm 0.008	0.184 \pm 0.005

1738 In Table 7, we report an augmented version of Table 4.4 with the concentration scores, assessing
 1739 sensitivity to the parameter k .

1740
 1741
 1742
 1743
 1744
 1745
 1746
 1747
 1748
 1749
 1750
 1751
 1752
 1753
 1754
 1755
 1756
 1757
 1758
 1759
 1760
 1761
 1762
 1763
 1764
 1765
 1766
 1767
 1768
 1769
 1770
 1771
 1772
 1773
 1774
 1775
 1776
 1777
 1778
 1779
 1780
 1781

1782

1783

1784

1785

1786

1787

1788

1789

1790

1791

1792

1793

1794

1795

1796

1797

1798

1799

1800

1801

1802

1803

1804

1805

1806

1807

1808

1809

1810

1811

1812

1813

1814

1815

1816

1817

1818

1819

1820

1821

1822

1823

1824

1825

1826

1827

1828

1829

1830

1831

1832

1833

1834

1835

Table 5: Full results across datasets.

Shapes3D			
model	InfoM \uparrow	InfoE \uparrow	InfoC \uparrow
AE	0.41 \pm 0.03	0.98 \pm 0.01	0.28 \pm 0.01
β -VAE	0.59 \pm 0.02	0.99 \pm 0.02	0.49 \pm 0.03
β -TCVAE	0.61 \pm 0.03	0.82 \pm 0.02	0.62 \pm 0.02
BioAE	0.56 \pm 0.02	0.98 \pm 0.01	0.44 \pm 0.02
AE (reproduction)	0.36 \pm 0.05	1.00 \pm 0.00	0.18 \pm 0.06
AE + ICA	0.78 \pm 0.02	1.00 \pm 0.00	0.42 \pm 0.09
<i>Discrete latent models</i>			
VQ-VAE	0.72 \pm 0.03	0.97 \pm 0.02	0.47 \pm 0.03
VQ-VAE w/ weight decay	0.80 \pm 0.01	0.99 \pm 0.01	0.46 \pm 0.02
QLAE	0.95 \pm 0.02	0.99 \pm 0.01	0.55 \pm 0.02
MPI3D			
model	InfoM \uparrow	InfoE \uparrow	InfoC \uparrow
AE	0.37 \pm 0.04	0.72 \pm 0.03	0.36 \pm 0.03
β -VAE	0.45 \pm 0.03	0.71 \pm 0.03	0.51 \pm 0.03
β -TCVAE	0.51 \pm 0.04	0.60 \pm 0.04	0.57 \pm 0.04
BioAE	0.45 \pm 0.03	0.66 \pm 0.04	0.36 \pm 0.03
AE (reproduction)	0.42 \pm 0.05	0.66 \pm 0.28	0.31 \pm 0.12
AE + ICA	0.44 \pm 0.12	0.66 \pm 0.28	0.31 \pm 0.14
<i>Discrete latent models</i>			
VQ-VAE	0.43 \pm 0.06	0.57 \pm 0.04	0.22 \pm 0.04
VQ-VAE w/ weight decay	0.50 \pm 0.04	0.81 \pm 0.04	0.41 \pm 0.04
QLAE	0.61 \pm 0.04	0.63 \pm 0.05	0.51 \pm 0.03
Falcor3D			
model	InfoM \uparrow	InfoE \uparrow	InfoC \uparrow
AE	0.39 \pm 0.03	0.74 \pm 0.03	0.20 \pm 0.03
β -VAE	0.71 \pm 0.05	0.73 \pm 0.04	0.70 \pm 0.03
β -TCVAE	0.66 \pm 0.02	0.74 \pm 0.04	0.71 \pm 0.04
BioAE	0.54 \pm 0.05	0.73 \pm 0.04	0.31 \pm 0.01
AE (reproduction)	0.37 \pm 0.14	0.75 \pm 0.01	0.21 \pm 0.06
AE + ICA	0.68 \pm 0.09	0.75 \pm 0.01	0.37 \pm 0.32
<i>Discrete latent models</i>			
VQ-VAE	0.61 \pm 0.04	0.83 \pm 0.05	0.42 \pm 0.02
VQ-VAE w/ weight decay	0.74 \pm 0.02	0.86 \pm 0.04	0.40 \pm 0.03
QLAE	0.71 \pm 0.03	0.77 \pm 0.02	0.44 \pm 0.02
Isaac3D			
model	InfoM \uparrow	InfoE \uparrow	InfoC \uparrow
AE	0.42 \pm 0.04	0.80 \pm 0.02	0.21 \pm 0.05
β -VAE	0.60 \pm 0.03	0.80 \pm 0.02	0.51 \pm 0.03
β -TCVAE	0.54 \pm 0.02	0.70 \pm 0.02	0.46 \pm 0.03
BioAE	0.63 \pm 0.03	0.65 \pm 0.03	0.33 \pm 0.04
AE (reproduction)	0.41 \pm 0.11	0.80 \pm 0.05	0.20 \pm 0.07
AE + ICA	0.64 \pm 0.17	0.80 \pm 0.05	0.34 \pm 0.05
<i>Discrete latent models</i>			
VQ-VAE	0.57 \pm 0.04	0.87 \pm 0.05	0.45 \pm 0.04
VQ-VAE w/ weight decay	0.73 \pm 0.03	0.81 \pm 0.03	0.44 \pm 0.04
QLAE	0.78 \pm 0.03	0.97 \pm 0.03	0.49 \pm 0.03

	Hyperparameter	Value
1836	is_unbalance	True
1837	learning_rate	0.05
1838	num_leaves	31
1839	feature_fraction	0.6
1840	reg_alpha	5.0
1841	reg_lambda	1.0
1842	min_gain_to_split	0.8
1843	min_data_in_leaf	30

Table 6: LightGBM hyperparameters used in all experiments.

Table 7: Sensitivity of concentration to k .

Model	Concentration (\uparrow)		
	$k = 25\%$	$k = 33\%$	$k = 50\%$
Base (none)	0.163	0.134	0.133
PCA	0.332	0.307	0.314
PCA + ICA	0.386	0.372	0.334
PCA + RandRot	0.287	0.280	0.235